Catalysis Science & Technology

Accepted Manuscript

ROYAL SOCIETY OF CHEMISTRY

www.rsc.org/catalysis

Journal Name

ARTICLE

Hexaaluminates: A review of the structure, synthesis and catalytic performances

Received 00th January 20xx,
Accepted 00th January 20xx

DOI: 10.1039/x0xx00000x

www.rsc.org/

M. Tian, X. D. Wang* and T. Zhang*

Hexaaluminates, a class of hexagonal aluminate compound, have peculiar layered structure consisting of alternatively stacked spinel block of closed packed oxide ions and mirror plane. These materials exhibit stable phase composition up to 1600 °C and exceptional resistance to sintering and thermal shock, which make them attractive catalysts for high-temperature applications. In this review, the structure of hexaaluminates is firstly introduced. Then we discuss recent advances in the synthesis and catalytic applications of metal-substituted or supported hexaaluminates such as catalytic combustion of CH_4, partial oxidation and CO_2 reforming of CH_4 to syngas and decomposition of N_2O with a special emphasis on the effect of chemical state of metals in the hexaaluminate framework on the catalytic performances. Finally, a brief summary and an outlook on some of the scientific challenges and suggestions of future investigations in the field are given.

1. Introduction

Hexaaluminates are a family of hexagonal aluminate compound and have peculiar layered structure consisting of alternatively stacked spinel block of closed packed oxide ions and mirror planes.[1] Its general formula can be presented as $AB_xAl_{12-x}O_{19}$, A being typically a mono-, di-, or trivalent large cations, for example A=Na, Ba, La, resident in the mirror plane. The component B represents transition-metal (Mn, Fe, Co, Cu, Ni, etc.)[2] or noble metal ions (Ir, Ru, Pd, Rh),[3, 4] which can partially or even completely substitute Al crystallographic sites. Although the crystal structure of hexaaluminates was deduced as being hexagonal with the composition of $LaAl_{12}O_{19}$ in as early as 1958,[5] the first catalytic studies on hexaaluminates was published in 1987, reporting the effect of additives such as BaO, SrO, and CaO on the surface area of oxide supports (Al_2O_3, ZrO, MgO) for catalytic combustion of methane.[6] The authors found that the mixing of BaO with Al_2O_3 at the composition of $(BaO)_{0.14}(Al_2O_3)_{0.86}$ maintained the largest surface area (20 m^2/g) above 1200 °C, which is attributed to the formation of barium hexaaluminate ($BaO{\cdot}6\ Al_2O_3$). When the cobalt oxide was supported on the barium hexaaluminate, the highest activity for the catalytic combustion of methane was obtained. Today, hexaaluminates are regarded probably as the most promising catalytic materials for high-temperature applications, such as catalytic combustion,[7] catalytic partial oxidation,[8] CO_2 reforming,[9] process-gas N_2O abatement,[10] and the decomposition of N_2O as a propellant.[11] This is mainly due to their exceptional thermal stability in combination with extraordinary capability to accommodate a variety of substituting and doping elements, allowing tailoring the properties to better targeting their applications. Since 1995, a considerable number of papers have been published in a wide variety field, including surface engineering[12], crystal chemistry,[13] structural chemistry[14] and heterogeneous catalysis[15-17], and is showing increasing tendency, as shown in Fig. 1.

In this review article, we summarize recent advances in the structure, synthesis method and catalytic performance of hexaaluminates. The following paragraph is devoted to the structure of hexaaluminates, with a focus on the introduction of β-Al_2O_3 and magnetoplumbite (MP) structures, defect mechanism and surface properties. Then, we discuss several typical synthesis methods of hexaaluminates and highlight the effect of preparation method on the specific surface area. The fourth section concerns the catalytic performances for combustion of CH_4, partial oxidation and CO_2 reforming of CH_4 to syngas, as well as decomposition of N_2O and discusses their correlation with microstructure of hexaaluminates. The main conclusion and outlook on some of the

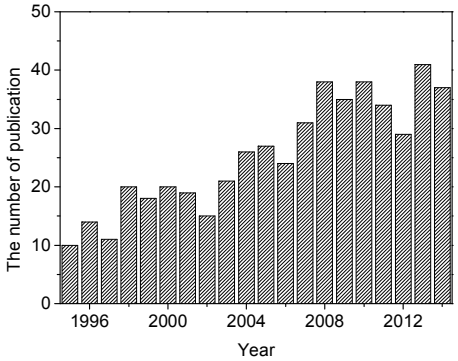

Fig. 1 Yearly number of papers on hexaaluminates since 1995 (searching in Web of Science).

State Key Laboratory of Catalysis, Dalian Institute of Chemical Physics, Chinese academy of Sciences, 116023, P. R. China. E-mail: taozhang@dicp.ac.cn; xdwang@dicp.ac.cn. *Electronic Supplementary Information (ESI) available: [details of any supplementary information available should be included here]. See DOI: 10.1039/x0xx00000x*

scientific challenges and further investigations for hexaaluminates as heterogeneous catalysts are presented at the end of the review. To be noted, hexaaluminates as monolith catalysts will not be dealt with in this review.

2. The structure of hexaaluminates

2.1 β-Al_2O_3 and magnetoplumbite (MP) structure

Hexaaluminates consist of the spinel block and mirror plane which are stacked alternatively to form a sort of layer structure, as shown in Fig. 2.[18] Spinel blocks are composed only of Al^{3+} and O^{2-} ions, having the same rigid structure as spinel. Large cations such as Na^+, K^+, Sr^{2+}, and La^{3+} are resided in the spacious mirror plane. Depending on the charge and radius of the large cations in the mirror plane, hexaaluminates have β-Al_2O_3 and magnetoplumbite (MP), respectively. Fig. 3 using layer by layer demonstration shows the difference between these two types of structures, e.g. β-Al_2O_3 has a large cation and an O^{2-} ions while MP has a large cation, three O^{2-} ions and an Al^{3+} ions in the mirror plane.[1] The hexaaluminates ($MAl_{12}O_{19}$; M=large cations) containing trivalent ions such as La^{3+} and divalent ions (M=Ca, Sr) usually have a crystal structure of the MP type [19, 20]. It was considered that barium hexaaluminate also has the same structure. However, Stevels et al.[21] found that it should have β-Al_2O_3 structure with the formula $Ba_{1-x}Al_{0.67+0.75x}O_{17+x}$(-0.2≤x≤0.35). Afterwards, Kimura et al.[22] revealed the existence of two compounds near the $BaO{\cdot}6Al_2O_3$ composition, which were tentatively denoted as barium hexaaluminate phase Ⅰ (Ba-poor) and phase Ⅱ (Ba-rich). Iyi et al. [19, 23] showed that barium hexaaluminate phase Ⅰ and phase Ⅱ have the composition of $Ba_{0.79}Al_{10.9}O_{17.14}$ and $Ba_{2.34}Al_{21.0}O_{33.84}$, respectively, and suggested that these were essentially of β-alumina structure based on the electron diffraction and crystallographic data. The hexaaluminates containing monovalent ions such as Na^+, K^+, Ag^+ also have β-alumina structure.[24-26] Iyi et al.[1] investigated the effect of large cations

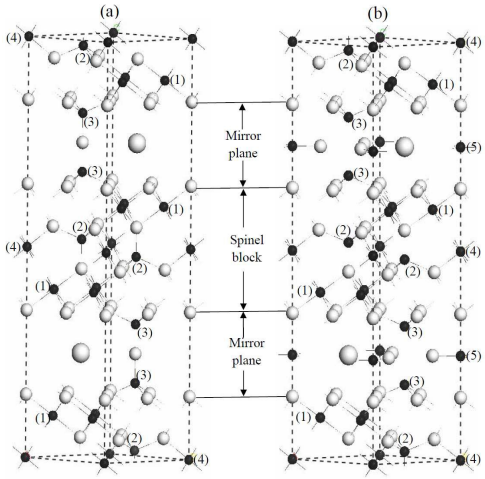

Fig. 2 The structure of hexaaluminate (a) β-Al_2O_3; (b) MP. ○Ba;○O; ●Al. Numbers in parenthesis refers to the different Al sites. Al(1), octahedral site; Al(2), tetrahedral site; Al(3) in β_l-Al_2O_3, tetrahedralsite; Al(3) in MP, octahedral site; Al(4), octahedral site; Al(5) in β_l-Al_2O_3, tetrahedral site; Al(5) in MP, trigonal bipyramid site.[18]

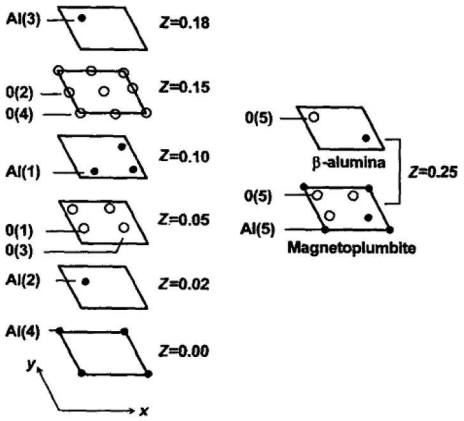

Fig. 3 Nomenclature of the atomic positions in β-Al_2O_3 and MP structures. Atoms are shown layer by layer. The mirror planes are at z=0.25, 0.75 and the centers of symmetry are at (0.5, 0.5, 0) and (0.5, 0.5, 0.5).[1]

radius on the bond lengths of M-O(2) and M-O(5) (Fig. 3) and found that the upper limit of large cations radius for MP type is 1.33 Å. The reason is as follows: The M-O(5) bond length increases slightly while the M-O(2) length does significantly with the radius of large cations, indicating that the large cations is in full contact with O(2) rather than with O(5). The difference between the lengths of M-O(2) and M-O(5) decreases with the enhancement of large cation size. As the M-O(5) length cannot change due to the repulsion between O(5) ions, the point where the lengths of M-O(5) and M-O(2) become equal can be expected to be the upper limit of the MP structure. This corresponds to an ionic radius of 1.33 Å. The large cations having radius less than 1.33 Å can enter either the β-alumina or the MP structure depending on their charge. The effect of the charge and radius of large cations on the hexaaluminate structure is summarized in Fig. 4.[1]

2.2 Charge compensation mechanism

The chemical formulae of β-Al_2O_3 and MP are ideally expressed as $MAl_{11}O_{17}$ and $MAl_{12}O_{19}$ (M: large cation), respectively. These stoichiometric expressions are only limited to a few MP compounds such as $CaAl_{12}O_{19}$ and $SrAl_{12}O_{19}$.[20] Non-stoichiometric composition has been observed for almost all β-Al_2O_3 and trivalent lanthanoid-ion-containing MP compounds.[19] Thus, the defect mechanism in the hexaaluminate structure is important. Roth et al.[27] and Wang et al.[28] proposed a complex Frenkel defect (or Reidinger defect) mechanism based on the neutron diffraction data and energy calculations. According to this mechanism, a pair of interstitial Al^{3+} ions which have migrated from spinel blocks by the Frenkel defect mechanism are bridged by an interstitial oxygen ion on the mirror plane. For example, in the barium hexaaluminate phase Ⅰ, the Al(1) shifts to the interstitial Al sites which are bridged by interstitial O ions so that the extra charge due to Ba ions can be compensated, as shown in Fig. 5. However, an interstitial oxygen and a barium ion simultaneous in the same mirror plane of a single cell is impossible due to the large ionic radius of both atoms compared with the distance of 2 Å between the Ba and interstitial oxygen sites. Therefore, one half unit cell contains a barium ion and has the

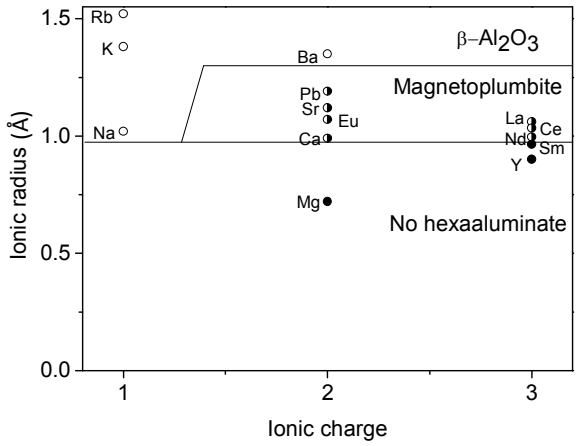

Fig. 4 The charge and ionic radius of large cations on the hexaaluminate structure.[1]

composition of "$BaAl_{11}O_{17}$" (Fig. 5(a)) with a charge of +1, and the other contains an interstitial oxygen with the defect of barium ion in the mirror plane owing to Frenkel defect of Al ions, the composition of which is "$OAl_{11}O_{17}$" (Fig. 5(b)) with a charge of -3. To attain charge neutrality, the molar ratio of these two types of half cell should be 3 to 1. Thus the formula of barium β-Al_2O_3 is necessarily $Ba_{0.75}Al_{11}O_{17.25}$. For La^{3+} ions containing MP, similar interstitial Al ions could be also detected, which results in the defect of La ions to avoid cation-cation interaction between La and interstitial Al ions. Thus, one type of half unit cell contains a La ion and has the composition of $LaAl_{12}O_{19}$ with charge +1. The other one contains La and Al(5) defects due to interstitial Al ions, with the composition of "$Al_{11}O_{19}$"having charge of -5. The ratio of the half unit cells should be 5 to 1 in order to attain the charge balance and the resulting chemical formula would be $La_{0.83}Al_{11.88}O_{19.0}$.

2.3 Thermal stability and surface structure of hexaaluminates

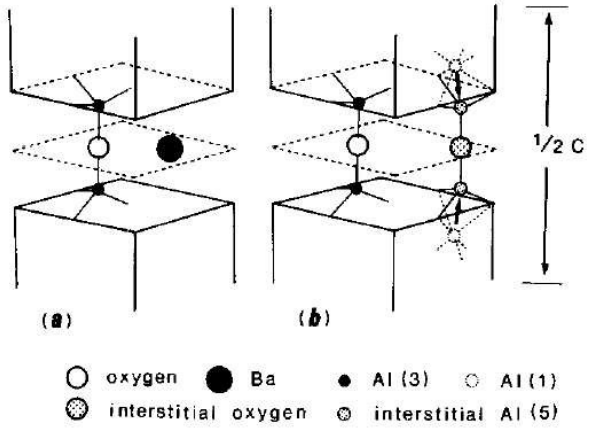

Fig. 5 Two types of half unit cell assumed to constitute barium β-Al_2O_3. (a) Half unit cell containing a Ba and an O ions in the mirror plane. (b) Half unit cell containing interstitial Al and O ions with the defect of Ba ion. The arrow indicates the shift of Al ions due to Frenkel defect mechanism.[19]

The specific surface area of hexaaluminates is around ~20 m^2/g after calcination at 1200 °C for several hours and it can still be retained to 10 m^2/g at 1600 °C, exhibiting excellent sintering-resistance.[7] TEM and SEM images of hexaaluminates (Fig. 6) present planar crystallites with particle size of 100-200 nm and thickness of 10-20 nm, indicating that the crystal growth along [001] direction is strongly suppressed.[29, 30] Machida et al.[30] found that diffusivity of oxide ions normal to c axis (⊥c) was an order of magnitude larger than those along c axis (∥c), indicating that the mirror plane is a preferential diffusion route of oxygen. As a result of anisotropic diffusion in the mirror plane, preferential grain growth of hexaaluminate along the ⊥c direction took place, as shown in Fig. 7. However, since such thin particles with the large aspect ratio (D/h in Fig. 6(d)) must be unstable because of increased surface energy, the particle size did not increase easily at elevated temperatures, thus leading to the reservation of large surface area.[30]

Surface exposed of catalysts is important for the adsorption and activation of reactants. Machida et al.[30] found that the reaction rate

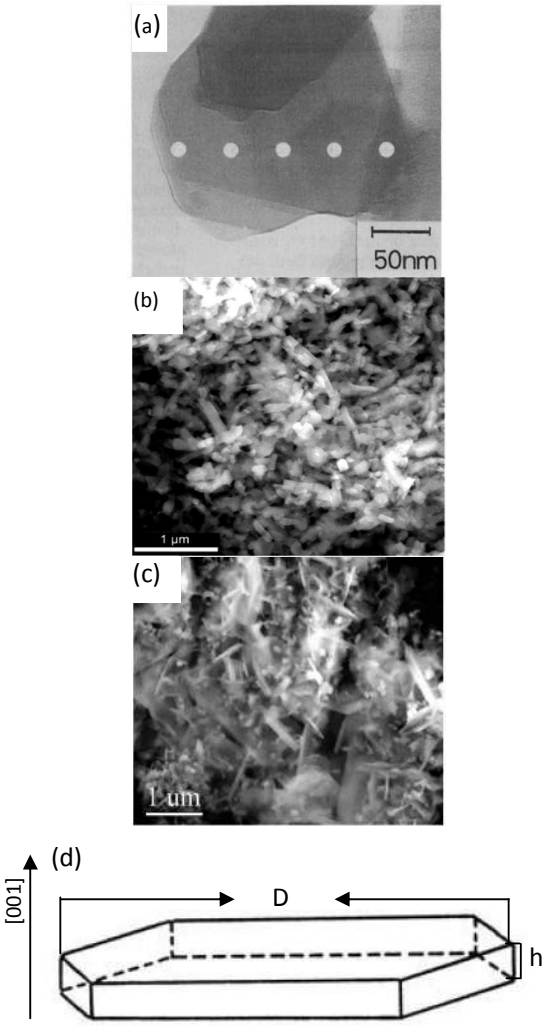

Fig. 6 TEM images of $BaAl_{12}O_{19}$ (a);[29] SEM images of $BaAl_{12}O_{19}$[31] (b) and $LaAl_{12}O_{19}$[32] (c); Schematic diagram of hexaaluminates microcrystal (d).[33]

for isotopic exchange ($^{18}O/^{16}O$) on (110) surface ($\perp$c) is larger than that on (001) surface ($\parallel$c) and deduced that the higher activity is attained on the side plane ($\parallel$ c) (Fig. 7) of hexaaluminate microcrystal rather than on the basal plane ($\perp$c) (Fig. 7). They also concluded that oxygen in the mirror plane preferentially participate in the adsorption and desorption during oxidation and reduction of Mn species in the hexaaluminate structure, which further confirmed the higher activity of side planes of hexagonal facet. Then modification of basal plane was conducted to enhance activity by depositing spinel Mn_3O_4 by air oxidation process. It was demonstrated that Mn_3O_4 completely covered the basal plane rather than side plane of hexaaluminate microcrystal. This was because the ionic configuration in the Mn_3O_4 spinel structure is analogous to that in the spinel block of hexaaluminats so that the basal plane surface could provide coherent interface with little stress, as presented in Fig. 8. On the other hand, Mn_3O_4 spinel/hexaaluminate side plane interface was so unstable due to a large misfit that coherency between these two phases was frustrated. Thus, coherent surface layer cannot be set up on the side plane of hexaaluminate microcrystals. This modified hexaaluminate showed higher specific activity for combustion of CH_4 as a result of promoting redox properties.

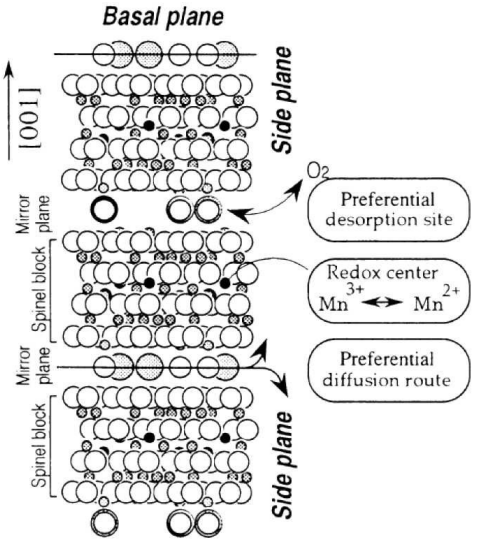

Fig. 7 Crystal structure and morphology of powder samples of Mn-substituted hexaaluminate.[30]

3. Synthesis methods

The hexaaluminates was first prepared from simple solid-state reaction in the 1980s.[6] The poor textural properties resulted from high crystallization temperature have to be improved for catalytic applications where an accessible surface plays a key role. Thus, the main efforts were made to increase the specific surface area of the solids, leading to the development of more efficient synthesis routes, such as sol-gel, co-precipitation, reverse microemulsion and so on. Table 1 summarized the effect of preparation method on the specific surface area of hexaaluminates.

3.1 Solid-state reaction

Solid-state reaction involves the calcinations of the metal oxide and carbonate as the starting materials through solid-state diffusion. Diffusion in the solid state is slow so that high reaction temperatures (typically higher than 1300 ^oC) and long reaction times are required to complete the reaction and obtain a pure hexaaluminate phase. Machida et al.[6] calcined the mixture of $BaCO_3$ and γ-Al_2O_3 and obtained pure β-Al_2O_3 phase at 1450 ^oC with surface area of 6 m^2/g. They found that $BaAl_2O_4$ is produced firstly from $BaCO_3$ and γ-Al_2O_3 followed by a reaction between $BaAl_2O_4$ and γ-Al_2O_3 to form hexaaluminates. Nugroho et al.[34] used mechanical activation methods concerning to the ball milling treatment before calcinations to improve the uniform mixing of the precursors and investigated the influence of precursors, milling regimes and calcination temperature on the composition and surface area. The most complete formation of $BaMnAl_{11}O_{19}$ at 1000^oC was observed in the systems of χ-Al_2O_3-BaO-MnO_2 precursors and the surface area is 7.7 m^2/g after calcination at 1300 ^oC. The solid-state reaction method is extremely simple and suitable for the production in large scale since the raw materials are inexpensive and easily obtained. However, this method produces inhomogeneity leading to the high formation temperature of hexaaluminates thus the low surface area.

3.2 Sol-gel

Several new synthesis routes, commonly classified as solution-mediated methods, were developed, such as sol-gel, co-precipitation, reverse microemulsion. These methods, based on dissolving precursors in a liquid media followed by drying and calcination steps, rapidly replaced solid−solid routes. Use of liquid media ensures a more homogeneous precursor, allowing decreasing the crystallization temperature by several hundreds of degrees, thus suppressing grain growth and loss of surface area.

Sol-gel method essentially bases on hydrolysis of precursors such as alkoxides, nitrates, carboxylates, acetylacetonates, chlorides, and other inorganics, to generate a homogeneous solution and transforming it into a gel by densification or subsequent heat

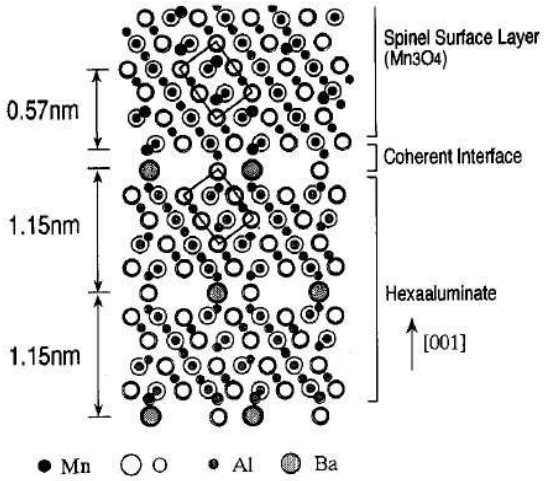

Fig. 8 Ideal interface of structures of Mn_3O_4 spinel/hexaaluminate.[30]

Table 1 The specific surface area of the hexaaluminate systems.

Systems	Preparation method	Raw materials	Calcination parameters			Surface area (m^2/g)	References
			T (^oC)[a]	t (h)[b]	A[c]		
Ba-Al	S[d]	$BaCO_3$, γ-Al_2O_3	1300	12	Air	6	6
	Sol-gel	alkoxide	1300	12	Air	9-13	6
			1200	24	Oxygen	9-11	35
			1200	5	Air	15	36
		Ba, alkoxide	1200	24	Oxygen	10	37, 38
	CP[e]	Nitrates, $(NH_4)_2CO_3$	1300	10	Air	10-15	16, 39-42
			1300	4	Air	9	43
			1200	4	Air	16	44
			1200	4	Air	51	45
			1200	4	Air	20	31
			1200	10	Air	25	10
			1200	5	Air	18	46
			1200	2	Air	24	47
		Nitrates, NH_4OH	1200	2	Air	38	47
			1200	4	Air	22	48
	RM[f]-FD[g] and SCD[h]	Alkoxide, isooctane(O[i]), polyethoxylated hexanol and 1-pentanol (Sf[j])	1300	4	Air	100-160	49-51
	RM	Alkoxide, isooctane(O), alcohole(Sf)	1300	/	/	15-25	8
	RM	Acetates, NH_4OH, cyclohexane(O), Triton X-100–n-hexanol(Sf)	1300	4	Air	90	52
Sr-Al	CP	Nitrates, $(NH_4)_2CO_3$	1300	10	Air	10	40
		Nitrates, $(NH_4)HCO_3$	1200	4	Air	18	44, 53
Sr-Mn	CP	Nitrates, $(NH_4)_2CO_3$	1200	5	Air	9	54
Ca-Al	CP	Nitrates, $(NH_4)_2CO_3$	1300	10	Air	9	40
		Nitrates, NH_4OH	1200	4	Air	14	55
Ca-Mn	CP	Nitrates, $(NH_4)_2CO_3$	1200	4	Air	17	56

$Sr_{0.8}La_{0.2}$-Mn	S	$MnCO_3$, $SrCO_3$, La_2O_3, and Al_2O_3	1200	5	Air	0.6	57
	Sol-gel	Sr, Alkoxide, nitrates	1200	5	Air	13-18	57-59
	CP	Nitrates, $(NH_4)_2CO_3$	1200	10	Air	10	60
			1200	4	Air	20-51	47, 61, 62
		Nitrates, NH_4OH	1200	4	Air	9	47
$La_{0.8}Sr_{0.2}$-Mn	CP	Nitrates, $(NH_4)_2CO_3$	1300	5	Air	9	63
$La_{0.8}Ce_{0.2}$-Al	CP	Nitrates, NH_4OH	1200	4	Air	16	55
$La_{1-x}Sr_x$-Mn (x=0.2, 0.4, 0.5, 0.6, 0.8)	CP	Nitrates, $(NH_4)_2CO_3$	1200	5	Air	3-25	54
$Sr_{0.3}Ba_{0.5}La_{0.2}$-Mn	CP	Nitrates, $(NH_4)_2CO_3$	1200	4	Air	29	61, 62
$Sr_{0.3}Ba_{0.5}La_{0.2}$-Mn	CP	Nitrates, $(NH_4)_2CO_3$	1100	4	Air	7	64, 65
$Sr_{1-x}Ln_x$-Mn(Ln=Ce,Pr,Nd,Sm, Gd;x=0,0.2,0.4,0.6,1)	Sol-gel	Sr, Alkoxide, nitrates	1200	5	Air	7-21	66
Ba-Cu_x(x=1, 2)	Sol-gel	Ba, Alkoxide, nitrates	1200	24	Oxygen	5-11	38, 67
Ba-Fe_x (2-4)	Sol-gel	Ba, Alkoxide, nitrates	1200	24	Oxygen	6-14	37
		Alkoxide, nitrates	1200	24	Oxygen	5-14	35
	CP	Nitrates, $(NH_4)_2CO_3$	1200	4	Air	16	68
Ba-Fe_x (2-12)	CP	Nitrates, $(NH_4)_2CO_3$	1200	4	Air	0-17	31
Ba-Fe	CP	Nitrates, $(NH_4)_2CO_3$	1200	10	Air	12	10, 69
			1200	4	Air	18	31, 68
Ba-Cr	CP	Nitrates, sulfate, $(NH_4)_2CO_3$, NH_4OH	1300	2	Air	17	70
Ba_xLa_{1-x}-Cr (x=0.25,0.5,0.75)	CP	Nitrates, sulfate, $(NH_4)_2CO_3$, NH_4OH	1300	2	Air	15-28	70
Ce_xBa_{1-x}-Mn (x=0.1-0.3)	RM-SCD	Nitrates, $(NH_4)_2CO_3$, cyclohexane(O), polyoxyethylene (6) tridecyl alcohol ether and n-hexanol(Sf)	1200	5	Air	26-74	71
Ba-Mn-Co	Sol-gel	Alkoxide, nitrates	1200	5	Air	14	36
Ba-Co	Sol-gel	Alkoxide, nitrates	1200	5	Air	14	36
Ba-Mn_x (x=2-4)	Sol-gel	Ba, Alkoxide, nitrates	1200	24	Oxygen	10-14	67
		Alkoxide, nitrates	1200	24	Oxygen	6-14	35

	CP	Nitrates, $(NH_4)_2CO_3$	1400	10	Air	12-17	42
	CP-SCD	Nitrates, $(NH_4)_2CO_3$	1200	4	Air	14-26	45
Ba-Mn	Sol-gel-SCD	Alkoxide, nitrates	1200	4	Air	72	72
	CP	Nitrates, $(NH_4)_2CO_3$	1300	/	/	15	73
			1200	10	Air	8	10
			1200	4	Air	21	18
			1200	2	Air	27	47
		Nitrates, NH_4OH	1200	2	Air	5	47
	CP-SCD	Nitrates, $(NH_4)_2CO_3$	1200	4	Air	38	45
	RM-SCD	Nitrates, $(NH_4)_2CO_3$, cyclohexane(O), polyoxyethylene (6) tridecyl alcohol ether and n-hexanol(Sf)	1200	5	Air	72	71
	RM	Nitrates, $(NH_4)_2CO_3$, cyclohexane(O), polyoxyethylene (6) tridecyl alcohol ether and n-hexanol(Sf)	1200	5	Air	43	71
Ba-$Mn_{0.5}$	CP	Nitrates, $(NH_4)_2CO_3$	1200	2	Air	24	47
		Nitrates, NH_4OH	1200	2	Air	23	47
Ba-Mg-Mn	Sol-gel	Acetate	1200	12	Oxygen	10	74
Ba-Fe-Mn_x (x=1-3)	Sol-gel	Alkoxide, nitrates	1200	24	Oxygen	4-15	35
Ba-Ni	CP	Nitrates, $(NH_4)_2CO_3$	1200	10	Air	17	10
La-$Mn_{0.5}$	CP	Nitrates, $(NH_4)_2CO_3$	1200	5	Air	27-31	54
La-$Mg_{0.5}$-$Mn_{0.5}$	CP	Nitrates, $(NH_4)_2CO_3$	1300	5	Air	12	63
	RM-SCD	Nitrates, $(NH_4)_2CO_3$, cyclohexane(O), polyoxyethylene(7) Octanyl phenyl alcohol ether and n-hexanol(Sf)	1200	5	Air	40	13
La-Mn	Sol-gel	Al_2O_3 sol, acetates	1200	6	Oxygen	21-42	75
		Acetate, alkoxide, nitrates	1400	1	Air	10	76
		Alkoxide, nitrates	1200	4	Oxygen	7-23	77
	CP	Nitrates, $(NH_4)_2CO_3$	1200	4	Air	25-41	78-80
	CP-SCD	Nitrates, $(NH_4)_2CO_3$	1200	2	Air	40	81
		Nitrates, NH_4OH	1200	2	Air	20	81

			1200	4	Air	28	82
	CP	Nitrates, NH_4OH	1200	4	Air	15	82
		Nitrates, $(NH_4)_2CO_3$	1200	/	Air	15	83, 84
			1200	4	Air	27	18, 84
			1200	5	Air	3-25	54
			1200	10	Air	12-14	10
			1300	5	Air	8.8-11.8	63
		Nitrates, NH_4HCO_3, NH_4OH	1200	4	Air	18	85
	RM-SCD	Nitrates, $(NH_4)_2CO_3$, cyclohexane(O), polyoxyethylene (7) Octanyl phenyl alcohol ether and n-hexanol(Sf)	1200	5	Air	30	13
La-Mn_x(x=2-4)	CP	Nitrates, NH_4HCO_3, NH_4OH	1200	4	Air	12-28	85
La-Mg	RM-SCD	Nitrates, $(NH_4)_2CO_3$, cyclohexane(O), polyoxyethylene (7) Octanyl phenyl alcohol ether and n-hexanol(Sf)	1200	5	Air	33	13
La-Mg_x-Mn_{1-x} (x=0.2, 0.8)	RM-SCD	Nitrates, $(NH_4)_2CO_3$, cyclohexane(O), polyoxyethylene (7) Octanyl phenyl alcohol ether and n-hexanol(Sf)	1200	5	Air	22-36	13
La-Fe	CP	Nitrates, $(NH_4)_2CO_3$	1400	4	Air	10	86
			1200	10	Air	18	10
		Nitrates, $(NH_4)_2CO_3$	1400	4	Air	10	32
	RM-SCD	Nitrates, $(NH_4)_2CO_3$ cyclohexane(O), AEO, Span 40 and n-pentanol(Sf)	1200	5	Air	46	87
La-Fe_5	CP	Nitrates, $(NH_4)_2CO_3$	1400	4	Air	8	86
La-Fe_x (x=2-12)	CP	Nitrates, $(NH_4)_2CO_3$	1400	4	Air	0-5	32
La-Cr	CP	Nitrates, sulfate, $(NH_4)_2CO_3$, NH_4OH	1300	2	Air	13	70
La-Co	CP	Nitrates, $(NH_4)_2CO_3$	1200	4	Air	24	84
La-Ni	CP	Nitrates, $(NH_4)_2CO_3$	1200	10	Air	28	10
Ba-Ni_x (x=0.25, 0.5, 1)	Sol-gel	Ba, Alkoxide, nitrates	1200	5	Air	24	88

Ba-Ni_x (x=0.2, 0.4, 0.6, 0.8, 1)	CP	Nitrates, $(NH_4)_2CO_3$	1400	1	Air	8-12	89
Ba-Mg	Sol-gel	Acetate	1200	12	Oxygen	13	74
Ba-M (M = Ru, Pd, Pt, Ni)	Sol-gel	Ba, Alkoxide, nitrates	1400	5	Air	2-12	4
La-Al	Sol-gel	Al_2O_3 sol, acetates	1200	6	Air	45	90
	CP-BM	Nitrates, $(NH_4)_2CO_3$	1200	10	Air	41	79, 80
	CP	Nitrates, $(NH_4)_2CO_3$	1200	4	Air	23	86, 91
			1200	10	Air	35	10
		Nitrates, $(NH_4)_2CO_3$	1400	4	Air	12	32
		Nitrates,NH_4HCO_3, NH_4OH	1200	4	Air	32	85
		Nitrates, $(NH_4)HCO_3$	1200	4	Air	22	44, 53
		Nitrates, NH_4OH	1200	4	Air	18	55
	RM-SCD	Nitrates, $(NH_4)_2CO_3$ cyclohexane(O), AEO, Span 40 and n-pentanol(Sf)	1200	5	Air	55	87
	Sol-gel	Alkoxide, nitrates	1200	4	Air	28	56
	CP	Nitrates, $(NH_4)_2CO_3$	1200	4	Air	17	56
La-Fe-Mn_x (x=0, 0.5, 1-5)	Sol-gel	Alkoxide, nitrates	1200	4	Oxygen	13-22	92
La-Mn-Fe_x(x=1, 2, 4, 6, 8)	CP	Nitrates, $(NH_4)_2CO_3$	1200	4	Air	6-21	91
$La_{0.8}M_{0.2}$-Mn (M=Ba, Ca, Sr, Y)	CP	Nitrates, $(NH_4)_2CO_3$	1200	4	Oxygen	17-20	93
$La_{0.95}Ba_{0.05}$-Mn	RM-SCD	Alkoxide, nitrates, isopropanol(O), n-butanol(Sf)	1200	2	Air	65	94
Ba-$Ir_{0.2}$-$Fe_{0.8}$	CP	Nitrates, $(NH_4)_2CO_3$	1200	4	Air	23	3, 95
Ba-$Ru_{0.2}$-Fe_x (x=0, 1)	CP	Nitrates, $(NH_4)_2CO_3$	1200	4	Air	19-31	96

[a]Temperature; [b]Time; [c]Atmosphere; [d]Solid state reaction; [e]Co-precipitation; [f]Reverse microemulsion; [g]Supercritical drying; [h]Freeze drying; [i]Oil phase; [j]Surfacant

treatment. It is one of the excellent methods by which to obtain fine particles of high purity oxides.[77] Another advantage is the low-temperature processing of complex oxides due to the homogeneous mixing of component at a molecular level thereby enhancing the specific surface area. Machida et al.[6] prepared Ba hexaaluminates using barium and aluminium isopropoxide as starting materials and obtained pure hexaaluminate phase at 1450 ^{o}C with surface area of 13 m^2/g. Even after calcination at 1600 ^{o}C for 5 h, the surface area still maintained 11 m^2/g. Particularly, hexaaluminate phase is directly obtained from the amorphous precursor without the formation of $BaAl_2O_4$ intermediates due to homogeneous mixing of Ba and Al atoms in the alcoholic solution. Woo et al.[59] investigated the effect of water content in the precursor solution on the thermal stability of $Sr_{0.8}La_{0.2}MnAl_{11}O_{19}$ and found that large amount of water (10 times of that of alkoxide) accelerated the sintering phenomena resulting in the rapid particle growth and drastic decrease of surface area. They attributed such decrease of surface as

increasing the amounts of water to the diffusion toward surface and enrichment of elements. Yan et al.[36] obtained aerogel- and xerogel-derived hexaaluminates by drying gels produced under supercritical conditions and ambient temperature and pressure, respectively, using barium ethoxide ($Ba(OC_2H_5)_2$) and aluminum sec-butoxide ($Al(OC_4H_9)_3$) precursors and ethanol solvent. It was found that aerogel-derived hexaaluminates have higher surface area, larger pore size and volume than xerogel-derived materials do, indicating that drying method significantly affected the properties of the hexaaluminates obtained. Xu et al.[72] investigated the effect of drying method on the phase composition and found that α-Al_2O_3 could be detected in the Xerogel calcined at 1200 ^oC (Xerogel-1200) while it was absent in the aerogel-1200 sample. The cause was as followed: In the conventional oven drying process, migration of the Ba, Mn, Al species due to the flowing of the liquid to the surface from the inner pores, driven by the gradient of capillary stress resulted in the heterogeneous mixing of the components since the solubility among Ba, Mn and Al species in water is different. With the supercritical drying, however, the migration of the Ba, Mn, and Al species caused by the flowing of the liquid could be avoided because the capillary stress is eliminated so that homogeneous mixing of the components could be maintained. Cho et al.[75] proposed surfactant-mediated synthesis of Mn-substituted hexaaluminate using environmentally benign surfactants such as Triton X-100, under ambient condition with a commercial alumina sol and metal acetate precursors. The ratio of Al_2O_3/surfactant and organic additives strongly influence the properties of hexaaluminates obtained. At Al_2O_3/cetyltrimethylammonium chloride (CTACl) ratio of 2.76, the surface area of $LaMnAl_{10}O_{18}$ sample calcined at 1200 ^oC for 6 h can be increased to 41.6 m^2/g when urea was used as an additive, compared to the one prepared without urea (28.7 m^2/g). Jana et al.[97] synthesized high purity lanthanum hexaaluminate powders by an advanced sol gel processing using cheaper precursors like boehmite ($Al_2O_3 \cdot H_2O$) and lanthanum nitrate. Combined with the addition of seeds ($LaAl_{11}O_{18}$) into the precursor solution, the formation temperature La-hexaaluminates (1201 ^oC) decreased by 99 ^oC by providing the sites for growth. As a result, near single phase lanthanum hexaaluminate formed at 1450 ^oC and pure phase at 1600 ^oC for 2 h.

Although the hexaaluminates prepared by sol-gel method have lower formation temperature and larger surface area, quite expensive raw materials and stringent reaction condition (oxygen and moisture-free) limits its wide application and is clearly not suitable for the production in large scale. Other alternatives for preparing hexaaluminates are desired.

3.3 Co-precipitation

The hexaaluminates are more often prepared by co-precipitation using carbonates route at the present. The precursors can be homogeneously mixed in the form of the ions and precipitated at the same time, which is favorable for their uniform dispersion in the solution. Compared with sol-gel method, the operation of co-precipitation is very simple and the raw materials are inexpensive and easily obtained. More importantly, the performances of hexaaluminates prepared by co-precipitation are comparable to those prepared by sol-gel method. In addition, pure hexaaluminates phase can be obtained at relatively lower temperature using co-precipitation than solid-state reaction.

Groppi et al.[42] firstly prepared $BaAl_{12}O_{19}$ and $BaMn_xAl_{12-x}O_{19}$ (x=0.5, 1, 2) samples by simple co-precipitation using $(NH_4)_2CO_3$ route. The authors claimed that the $BaAl_{12}O_{19}$ hexaaluminate has the surface area of 15 m^2/g calcined at 1300 ^oC, compared to those prepared via the hydrolysis of alkoxides even if the formation of $BaAl_2O_4$ as intermediate was observed, indicating $BaAl_2O_4$ did not prevent obtaining a final material with high surface area. Jang et al.[47] investigated the synthesis of various hexaaluminates prepared by aqueous $(NH_4)_2CO_3$ and NH_4OH precipitation methods using supercritical drying and found that the surface area of hexaaluminates synthesized by the $(NH_4)_2CO_3$ co-precipitation method, in general, is much higher than those synthesized by the NH_4OH co-precipitation. For example, the surface area of $Sr_{0.8}La_{0.2}MnAl_{11}O_{19}$ synthesized by $(NH_4)_2CO_3$ is 50.8 m^2/g versus 8.8 m^2/g when synthesized by NH_4OH co-precipitation. Besides the precipitator, precipitation temperature also greatly affected the properties of hexaaluminates. It was generally accepted that the surface area increased with the precipitation temperature up to 60 ^oC and changed slightly further enhancing the precipitation temperature.[98] Zheng et al.[99] studied the effect of amount of $(NH_4)_2CO_3$ on the phase composition and surface area and indicated that the optimum ratio of $(NH_4)_2CO_3$/metal precursors is 1.5.

3.4 Reverse microemulsion

Reverse microemulsion is an efficient method to prepare hexaaluminate nanocrystals with high specific surface area. Fig. 9 showed the diagram of reverse microemulsion synthesis of hexaaluminates.[13] In this technique, nanometre-sized aqueous micelles dispersed in an oil phase are used as nanoreactors for controlled hydrolysis and condensation of metal alkoxide. Unlike conventional sol-gel and co-precipitation processing, the reaction rate in this approach is controlled by the diffusion of precursors from the oil phase to the aqueous domains, instead of the hydrolysis of one of the precursors. Despite the different hydrolysis rates of metal alkoxides, chemical homogeneity can be attained with the mediation of the reverse microemulsion since the alkoxides have similar diffusivities in the oil phase. In the spite of the high specific surface area of targeted hexaaluminates obtained by this method, the metal precursors, surfactant and organic phase used are not environmental-friendly and their cost is high. In addition, the preparation is difficult to operate leading to poor reproducibility and the yield is very low.

The discrete barium hexaaluminate nanoparticles were firstly prepared using sol-gel processing in reverse microemulsions in 2000 by Zarur et al.[49-51]. By carefully control synthesis parameters such as the composition of the reverse microemulsion, water to alkoxide ratio, aging time, powder recovery and drying techniques, the particle size and specific surface area of final Ba-hexaaluminate after calcination at 1300

°C is 30 nm and 160 m^2/g, respectively. Such a specific surface area is regarded to be the largest for hexaaluminate catalysts so far. From then on, a variety of metal-substituted hexaaluminates with high surface area were successfully synthesized by modifying the synthesis parameters such as composition of microemulsion, aging time and drying techniques. For example, Sahu et al.[52] used cyclohexane as the oil phase, Triton X-100-n-hexanol as surfactant cosurfactant mixture and barium acetate and NH_4OH as aqueous phase. Barium hexaaluminate nanowhiskers were finally synthesized with the specific surface area of 90 m^2/g due to the Triton X-100 acted as a soft template for the formation of nanowhiskers. Teng et al.[94] developed a novel microemulsion system, consisting of water, iso-propanol and n-butanol to synthesize the nanostructure $La_{0.95}Ba_{0.05}MnAl_{11}O_{19}$ catalyst with the surface area of 65 m^2/g. The same author prepared $Ce_xBa_{1-x}MnAl_{11}O_{19}$ (x=0.1-0.3) catalysts with the surface area of 25 to 74 m^2/g by the reverse microemulsion using the nontoxic and inexpensive inorganic salts, instead of the alkoxide as reactants[71].

In addition, Jiang et al.[87] also used inorganic $(NH_4)_2CO_3$ precipitant and metal nitrate precursors to prepare Fe-substituted hexaaluminates with the surface of area of 45 m^2/g. Now, extensive efforts have been made to simplify the operation and use nontoxic and inexpensive agents and reactants for the reverse microemulsion to synthesize hexaaluminates with high performance.

Besides the preparation method mentioned above, other methods such as the decomposition of nitrates,[100-107] hydrothermal synthesis,[81] alumoxane method,[108, 109] gel-to-crystallite conversion method,[110] carbon-templating,[111, 112] activated reactive synthesis,[15, 113-115] freeze drying method,[116, 117] and solution combustion synthesis[63] were also used by researchers to synthesize a variety of metal-substituted hexaaluminates. The decomposition of nitrates method is extremely simple, just adding aqueous solutions to a polyethylene glycol-isopropyl alcohol one, following drying and calcination at appropriate temperature. Moreover, the surface area obtained is comparable to that prepared by sol-gel and co-precipitation methods at similar synthesis conditions. However, it is still difficult to obtain high surface hexaaluminate catalysts by this method mainly due to the inhomogeneous mixing of precursors. Carbon templating method involves the impregnation of carbon with concentrated solutions of the metal cations followed by drying and thermal treatment. The

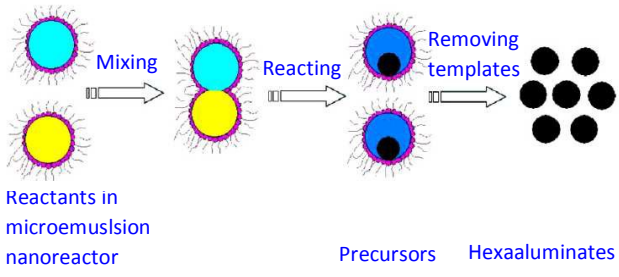

Fig. 9 Diagram of Reverse microemulsion synthesis of hexaaluminates.[13]

largest surface area reported at the present is 102 m^2/g for $BaAl_{12}O_{19}$ using this method by combusting carbon after the formation of hexaaluminate, which is lower than that reported using reverse micro-emulsion methods. Advantageously, carbon templating route is more suitable for practical implementation due to its versatility, simplicity and scalability. Activated reactive synthesis (ARS) is a new solvent free synthesis method to prepare high surface mixed oxides. It usually consists of three consecutive steps: (⍰) preparation of micrometric hexaaluminate parent material by solid state reaction; (⍰) crystal size (~20 nm) reduction step by grinding at high energy; (⍰) nanocrystal deagglomeration to enhance the surface area by grinding at low energy. ARS is easy to scale-up (60 g batches) without using expensive waste treatments and sophisticated process control as in the case of applying microemulsion combined with freeze drying processes. However, surface contamination originated from the grinder cannot be avoided.

Although significant progress has been made, synthesis of high-surface hexaaluminates as catalysts or catalyst supports using simple, cost-effective and environmental benign method is still challenging due to high crystallization temperature.

4. Catalytic performances

Metal-substituted hexaaluminates have become of great interest for some high-temperature catalytic applications, such as catalytic combustion of CH_4, partial oxidation of CH_4, CO_2 reforming of CH_4 and decomposition of N_2O, due to their exceptional resistance to sintering and thermal shock.[6, 30, 118-124] Fig. 10 summarized the catalytic applications of hexaaluminates. In addition, introducing different metal cations and large cations into the framework of hexaaluminates can generate a variety of chemical compositions and significantly influence their catalytic performances. In the following sections, the catalytic performances of hexaaluminates and their correlation to the microstructure will be discussed in detail.

4.1 Catalytic combustion of CH_4

Catalytic combustion of methane is considered as a promising alternative to conventional thermal combustion for energy production due to the decrease in the emission levels of noxious and/or greenhouse effect gases (NO_x) in the atmosphere[125]. In order to attain a high energy transforming efficiency and low emissions of air pollutants, a catalyst with excellent ignition activity and high resistance to sintering is urgently desired. Arai et al.[118] examined the activity of $BaMAl_{11}O_{19}$ (M=Cr, Mn, Fe, Co, Ni) for combustion of CH_4 and found that all the metal-substituted hexaaluminates exhibited higher activity than un-substituted $BaAl_{12}O_{19}$ catalyst. Among them, Mn-substituted hexaaluminates was the most active with the $T_{10\%}$ of 540 °C and $T_{90\%}$ of 740 °C. Since then, lots of studies on the improvement of activity and reaction mechanism of combustion of CH_4 over hexaaluminates have been reported. Table 2 summarized the catalytic performances of some metal substituted and supported hexaaluminates for combustion of CH_4.

Journal Name

ARTICLE

4.1.1 Reaction mechanism. Reaction mechanism of catalytic combustion of CH_4 over hexaaluminates involves a Mars-van Krevelen redox cycle where the adsorbed substrate is re-oxidized by bulk oxygen rather than oxygen coming from the gaseous phase. Thus, catalytic combustion of CH_4 can be described with the following equations:[126]

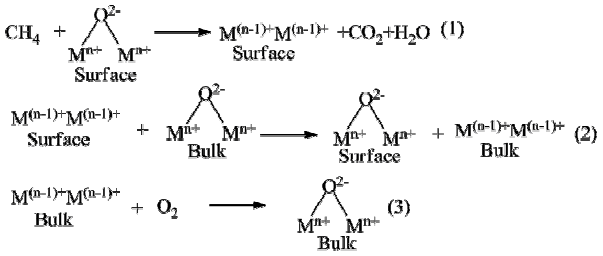

In the first step, CH_4 is reduced by surface active oxygen resulting in the formation of CO_2, H_2O and surface reduced sites. This step is followed by the diffusion of oxygen ions from the bulk to the surface reduced sites. Finally, the original hexaaluminate is regenerated by the gaseous phase oxygen. According to the above reaction mechanism, both the reducibility of metal ions and the mobility of lattice oxygen in the hexaaluminates will significantly influence their catalytic performance.

4.1.2 Metal-substituted hexaaluminates. Among the transition metal-substituted hexaaluminated studied, Mn-substituted samples have been investigated most and also exhibited the highest activity for combustion of CH_4. Bellotto et al.[41] identified the chemical state of Mn ions in the $BaMn_xAl_{12-x}O_{19-\alpha}$ (x=0.5, 1-3) hexaaluminates by means of X-ray absorption spectroscopy and X-ray powder diffraction structure refinements of multiple diffraction powder data sets. At low loading (up to x=1), Mn preferentially entered tetrahedral Al(2) sites of Ba-β_l-Al_2O_3 as divalent cation. The occupancy of Ba sites in the mirror planes acts as a charge compensation mechanism to balance substitution of Al^{3+} with Mn^{2+}. At high Mn loading (x≥1), the occupation of Ba sites reaches unity and Mn preferentially entered octahedral Al(1) sites as Mn^{3+}. However, the incorporation of Mn^{3+} in the octahedral Al(1) sites causes reduction of surface area and has no beneficial effect on catalytic activity. Different from the results obtained by Bellotto et al., Artizze-Duart et al.[35, 67] speculated that the activity increased with Mn content and the highest activity was obtained for catalysts containing 3 Mn. They also discovered that incorporation of Mn in excess (x>3) led to another phase formation (manganese oxide or spinel), which was responsible

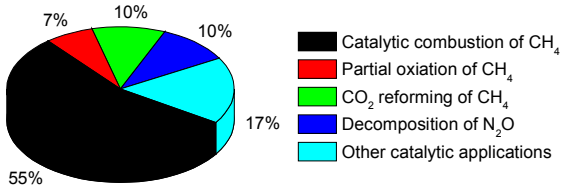

Fig. 10 Summary of the catalytic applications of hexaaluminates (Searching in Web of Science).

for the decrease in activity of hexaaluminate with 4 Mn. Groppi et al.[127] found that the introduction of Mg ions into $LaMnAl_{11}O_{19}$ resulted in a higher specific catalytic activity per Mn mol. Such a behavior should be associated with the stabilization of Mn ions at high oxidation state, generally considered as active sites, due to the co-presence of Mg^{2+}. Jang et al.[47] reported that $LaMnAl_{11}O_{19}$ was much more active than the $BaMnAl_{11}O_{19}$, and they ascribed the activity enhancement to the different oxidation state of Mn ions in the two types of hexaaluminates. Li and Wang[128] prepared Mn-substituted Ba-La-hexaaluminate rod-like nanoparticles and found that $Ba_{0.2}La_{0.8}MnAl_{11}O_{19}$ catalyst exhibited much higher activity than either $BaMnAl_{11}O_{19}$ or $LaMnAl_{11}O_{19}$. Evidently, both the substitution degree and the nature of large cations in the mirror plane significantly affected the Mn^{2+}/Mn^{3+} redox cycle, and then the catalytic performance.

Fe has been also reported as efficient promoters for catalytic combustion of CH_4. In contrast to Mn, which only substituted for a very limited number of Al ions, and excess Mn existing as catalytically inactive Mn oxides outside the hexaaluminate framework, Fe could completely replace Al and lead to the formation of a $BaFe_{12}O_{19}$ hexaferrite structure. Groppi et al.[129] prepared $BaFe_xAl_{(12-x)}O_{19}$ samples (x=1, 3, 6, 9, 12) and claimed that $BaFe_{12}O_{19}$ calcined at 700 °C was very active in CH_4 combustion but it deactivated both upon increasing the calcination temperature and upon treatment at 900 °C under reaction conditions. The observed deactivation phenomenon could be associated both with sintering and with a partial Fe^{3+} to Fe^{2+} reduction. Upon calcination at 1300 °C, $BaFe_6Al_6O_{19}$ showed the best catalytic properties among $BaFe_xAl_{(12-x)}O_{19}$. However, its activity is lower than that of Mn-substituted hexaaluminates. Naoufal et al.[37] reported that Fe^{3+} ions occupied the octahedral S1 and S2 sites in $BaFeAl_{11}O_{19}$ and when Fe/Ba = 2-4, Fe^{3+} ions entered into two new octahedral sites (S3 and S4). Fe^{3+} in the former two octahedral sites likely accounted for the increase in the intrinsic activity with Fe content. Laassiri et al.[114] used an activated reactive synthesis (ARS) to prepare nano $BaM_xAl_{12-x}O_{19-\delta}$ (M=Mn, Fe, Co, x=1, 2) hexaaluminates and discovered that Mn-containing materials were more active than Fe- and Co-

Journal Name

ARTICLE

Table 2 Catalytic performances of hexaaluminates for combustion of CH_4

Catalysts	Surface area (m^2/g)	Reaction conditions	$T_{10\%}$ (°C)	$T_{90\%}$ (°C)	E_a(kJ/mol)	Reaction rate ($mol \cdot m^{-2} h^{-1}$)[a]	References
Ba-Al	15	1 % CH_4,99 % air, GHSV: 48000 h^{-1}	700	>850	/	/	41
	15	1 % CH_4,99 % air, GHSV: 48000 h^{-1}	710	845	/	$<6\times10^{-6}$	36
	51	1 % CH_4,99 % air, GHSV: 50000 h^{-1}	624	750	/	/	45
	9-11	0.5 % CH_4,4 % O_2, GHSV: 15000–25000 h^{-1}	700	800	/	0.35×10^{-6}	35
	10	1% CH_4,4 % O_2, GHSV: 15000–25000 h^{-1}	675	780	120	1.98×10^{-6}	38
	100	0.5 % CH_4,20 % O_2, GHSV: 18 L $h^{-1}g^{-1}$	620	/	/	4×10^{-5} [b]	114
Ba-Mn	10	0.5 % CH_4,4 % O_2, GHSV: 100000 h^{-1}	530	720	/	/	43
Ba-Mn	72	1 % CH_4,99 % air, GHSV: 48000 h^{-1}	450	630	/	/	72
	16		600-745	755	/	2.4×10^{-5} [c]	36
Ba-Mn_x(x=0.5,1-3)	6-20	1 % CH_4,99 % air, GHSV: 48000 h^{-1}	550-600	750-800	88-97	2.9×10^{-4}-1.2×10^{-3} [d]	41
Ba-Mn_x(x=1-4)	10-20	0.5 % CH_4,4 % O_2, GHSV: 20000–25000 h^{-1}	420-470	660-750	/	0.04-0.11	67
	6-20	0.5 % CH_4,4 % O_2, GHSV: 15000–25000 h^{-1}	425-470	670-730	/	$2.5\text{-}6\times10^{-5}$	35
	14-38	1 % CH_4,99 % air, GHSV: 50000 h^{-1}	512-534	676-720	/	/	45
Ba-Mn_x(x=1,2)	60-71	0.5 % CH_4,20 % O_2, GHSV: 18 L $h^{-1}g^{-1}$	500-545	/	/	$2.6\text{-}3.6\times10^{-4}$ [b]	114
Ba-Mg	13	1 % CH_4,4 % O_2, GHSV: 6.4 L $h^{-1}g^{-1}$	597	757	157	/	74
Ba-Mg-Mn	10	1 % CH_4,4 % O_2, GHSV: 6.4 L h^{-1} g^{-1}	462	717	86	/	74
Ba-$Mn_{0.5}Co_{0.5}$	14	1 % CH_4,99 % air, GHSV: 48000 h^{-1}	585	740	/	4.2×10^{-5} [c]	36
BaFe_x(x=1-4)	5-14	0.5 % CH_4,4 % O_2, GHSV: 15000–25000 h^{-1}	495-520	670-730	79-92	$2.8\text{-}6.4\times10^{-5}$	35
Ba-Fe_x(x=1,2)	74-78	0.5 % CH_4,20 % O_2, GHSV: 18 L $h^{-1}g^{-1}$	527-553	/	/	$1.7\text{-}2.4\times10^{-4}$ [b]	114
Ba-$FeMn_x$(x=1-3)	4-15	0.5 % CH_4,4 % O_2, GHSV: 15000–25000 h^{-1}	440-460	670-705	80-85	$5\text{-}8\times10^{-5}$	35
Ba-Cu_x(x=1-2)	5-11	0.5 % CH_4,4 % O_2, GHSV: 20000–25000 h^{-1}	480-510	720-760	/	0.06	67
	11	1 % CH_4,4 % O_2, GHSV: 15000–25000 h^{-1}	510	740	85-98	$5.90\text{-}8.70\times10^{-5}$	38
Ba-Co	79	0.5 % CH_4,20 % O_2, GHSV:	568	/	/	8×10^{-5} [b]	114

		18 L $h^{-1}g^{-1}$					
Ba-Co	14	1 % CH_4,99 % air, GHSV: 48000 h^{-1}	660	815	/	<6×10^{-6} [c]	36
La-Al	/	1 % CH_4,99 % air, GHSV: 40000 h^{-1}	620	810	/	/	82
	23	1 % CH_4,99 % air, GHSV: 50000 h^{-1}	620	770	/	/	91
	24-55	1 % CH_4,4 % O_2, GHSV: 6L $h^{-1}g^{-1}$	550-620	635-775	/	/	87
	7-23	1 % CH_4,99 % air, GHSV: 50000 h^{-1}	630	798	/	/	77
	67	1 % CH_4,4 % O_2, GHSV: 50000 h^{-1}	625	780	/	/	130
$LaMn_{0.5}$	43	1 % CH_4,99 % air, GHSV: 40000 h^{-1}	515	710	/	/	82
La-Mn	21-42	1 % CH_4,99 % air, GHSV: 48000 h^{-1}	490	720	/	1.3×10^{-3}	75
	7-22	1 % CH_4,99 % air, GHSV: 50000 h^{-1}	452-546	579-664	/	/	77
	30	1 % CH_4,99 % air, GHSV: 48000 h^{-1}	460	750	/	/	13
	28	1 % CH_4,99 % air, GHSV: 40000 h^{-1}	450	670	/	/	82
	20-40	1 % CH_4,99 % air, GHSV: 40000 h^{-1}	445-500	645-725	/	/	81
	18	1 % CH_4,4 % O_2, GHSV: 50000 h^{-1}	620	790	/	/	85
	20	1 % CH_4,4 % O_2, GHSV: 50000 h^{-1}	510	735	/	/	131
	15	1 % CH_4,99 % air, GHSV: 54000 h^{-1}	480	690	87-94	/	127
La-Mn_x(x=2-3,6)	7-20	1 % CH_4,99 % air, GHSV: 40000 h^{-1}	440-450	680-720	/	/	82
La-Mn_x(x=2-4)	12-28	1 % CH_4,4 % O_2, GHSV: 50000 h^{-1}	480-590	740-820	/	/	85
La-$MnFe_x$(x=1,2,4,6,8)	6-17	1 % CH_4,99 % air, GHSV: 50000 h^{-1}	470-590	680-790	/	/	91
La-Fe-Mn	37	1 % CH_4,4 % O_2, GHSV: 50000 h^{-1}	480	680	/	/	130
La-Mg	33	1 % CH_4,99 % air, GHSV: 48000 h^{-1}	570	850	/	/	13
La-$Mg_{0.5}Mn_{0.5}$	15	1 % CH_4,99 % air, GHSV: 54000 h^{-1}	480	670	87-94	/	127
	40	1 % CH_4,99 % air, GHSV: 48000 h^{-1}	460	690	/	/	13
$La_{0.8}A_{0.2}$-Mn(A=Ba,Ca,Sr,Y)	17-20	1 % CH_4,99 % air, GHSV: 50000 h^{-1}	508-538	620-676	/	/	93
La-Fe	22	1 % CH_4,99 % air, GHSV: 50000 h^{-1}	554	815	/	/	92
	12-46	1 % CH_4,99 % air, GHSV: 6L $h^{-1}g^{-1}$	400-505	495-654	/	/	87
La-Fe_2	15	1 % CH_4,4 % O_2, GHSV: 50000 h^{-1}	510	710	/	/	130
La-$FeMn_x$(x=0.5,1-5)	13-18	1 % CH_4,99 % air, GHSV: 50000 h^{-1}	497-602	701-878	/	/	92
$Sr_{0.8}La_{0.2}$-Mn	20	1 % CH_4,99 % air, GHSV: 48000 h^{-1}	542	735	/	/	62
	20		530	740	/	/	61

	9	1 % CH_4,99 % air, GHSV: 70000 $cm^3 h^{-1}g^{-1}$	550	/	/	/	47
$Sr_{0.3}Ba_{0.5}La_{0.2}$-Mn	29	1 % CH_4,99 % air, GHSV: 48000 h^{-1}	535	733	/	/	62
			530	760	/	/	61
$Sr_{1-x}Ln_x$(Ln=Ce,Pr,Nd,Sm,Gd; x=0,0.2,0.4,0.6,1))-Mn	6-21	1 % CH_4,99 % air, GHSV: 48000 h^{-1}	500-570	770-870	/	/	66
A-Mn(A=K,Ca)	17-28	1 % CH_4,99 % air, GHSV: 50000 h^{-1}	490-525	670-722	/	/	56
$Ba_{1-x}La_x$-Cr(x=0,0.25,0.45,0.75,1)	13-27	1 % CH_4,99 % air, GHSV: 2.5L $h^{-1}g^{-1}$	480-571	/	/	/	70
15%$(Mn_{1-x}M_x)_3O_4$/Ba-Mn(M=Fe,Co,Ni;x=0,0.2,0.4,0.6,0.8,1)	13[e]	2 % CH_4,98 % air, GHSV: 6000 $cm^3 h^{-1}g^{-1}$	340-420	520-610	/	/	30, 33
1.44%Pd/$Sr_{0.8}La_{0.2}$-Mn	/	1 % CH_4,20 % O_2, GHSV: 48000 h^{-1}	450	700	/	/	132
2%Pd/$Sr_{1-x}La_x$-Mn(x=0,0.4,1)	11-14	1 % CH_4,99 % air, GHSV: 70000 $cm^3 h^{-1}g^{-1}$	360-450	/	106	/	47
10%CeO_2/Ba-Al	160[e]	1 % CH_4,99 % air, GHSV: 60000 h^{-1}	400	560	145	/	51
1%Pd/$Sr_{0.3}La_{0.2}Ba_{0.5}$-Mn	19[e]	1%CH_4,4%CO_2, 4%H_2O,18.2%O_2,GHSV: 415000 h^{-1}	600	/	113-116	4.4×10^{-6}-1.6×10^{-5} [d]	133
1%Pd/(60%$Sr_{0.3}La_{0.2}Ba_{0.5}$-Mn+40%Al_2O_3)	51	1%CH_4,4%CO_2, 4%H_2O,18.2%O_2,GHSV: 415000 h^{-1}	500	680	114	2.8×10^{-4} [d]	64
1.5%Pd/La-Mn	13-15	1 % CH_4,99 % air, GHSV: 1000-24000 h^{-1}	/	395-600	65-99	/	83

[a]Intrinsic activity (mol CH_4 converted per hour and per square meter) at 500 °C (<20% CH_4 conversion); [b]Intrinsic activity at 600 °C (<20% CH_4 conversion); [c]Intrinsic activity at 550 °C (<20% CH_4 conversion); [d] Calculated based on the intrinsic activity at 600 °C and the corresponding activity energy reported in References 41, 64 and 133 using Arrhenius equation; [e]The specific surface area of support

containing ones and the increase in transition metal content was beneficial to the catalytic activity. They employed several characterization techniques to clarify the reason why the activity was improved and the results were summarized in Fig. 11. Different from Mn-substituted hexaaluminates wherein activity enhancement was parallel with Mn surface and reducible Mn content as well as the oxygen mobility (Fig. 11 (a)), the increase in specific activity of Fe-containing hexaaluminates was not accompanied by the rise of all parameters (Fig. 11 (b)). This indicated that multiple factors including oxygen transfer properties and transition metal valence and concentration on the surface determined the catalytic properties of the nano-hexaaluminates.

Besides more active Mn and Fe, Co,[2, 36, 84, 114] Cu,[38, 67] Mg,[13, 74, 127] Ni,[2] Cr,[2, 70] Ru and Pt[4]-substituted hexaaluminates were also reported for combustion of CH_4. Compared with Mn and Fe, the substitution degree of these metals is relatively low, generally less than 2 metal ions, which accounted for their limited activity improvement for combustion of CH_4. In particular, only quite a little amount of noble metal (less than 0.2 metal ions) can enter the lattice of hexaaluminates due to their much larger ion radius than Al^{3+}. Remarkable sintering of noble metals outside of framework is observed so that the activity is usually poor even lower than that of transition metals-substituted hexaaluminates.[3, 95] Thus, few studies were reported on combustion of CH_4 over noble metals-substituted hexaaluminates.

4.1.3 Metal-supported on hexaaluminates. The investigation of hexaaluminates supported metals for combustion of CH_4 mainly focuses on supported Pd catalysts, which show excellent ignition activity for combustion of CH_4. Sekizawa et al.[132] investigated the

catalytic performances of $Pd/Sr_{0.8}La_{0.2}XA_{11}O_{19}$ (X = Al and Mn) and found that the activity of Pd/ $Sr_{0.8}La_{0.2}A_{12}O_{19}$ initially increased with temperature but decreased at high temperature (ca. 700 °C), which was associated to the sintering of Pd particles due to the dissociation of PdO into metallic Pd. Such significant drop in catalytic activity can be avoided by the use of Mn-substituted hexaaluminate (X = Mn) as a catalyst support, due to its activity for combustion. Sohn et al.[58] studied the evolution of chemical state of Pd with the calcination temperature and demonstrated that PdO on $Sr_{0.8}La_{0.2}MnAl_{11}O_{19}$ (SLMA) was dissociated to metallic Pd after calcination at 1000 °C. Furthering increasing calcination temperature to 1200 °C led to the formation of $Pd^{\delta+}$ species due to strong interaction of Pd^0 and SLMA. Baylet et al.[64, 65] compared catalytic activity and stability of Pd/Mn-substituted hexaaluminates to those of Pd/Al_2O_3 reference sample and found that Pd/Al_2O_3 showed the highest activity but progressively deactivated due to the decomposition of PdO to metal Pd. In the case of Pd/Mn-substituted hexaaluminates, an oxygen transfer from oxidized manganese sites to reduced palladium sites occurred to avoid the reduction of PdO to Pd (Fig. 12) thus excellent stability was obtained. This clearly showed the beneficial effect of the support for the stabilization of the PdO active phase at high reaction temperature. They also reported that the effect of the palladium precursor salt on the catalytic activity and stability.[133] It was observed that the samples prepared using $Pd(acac)_2$ as palladium source presented higher palladium dispersion (i.e. smaller crystal sizes, 2-3 nm calcined at 650 °C), and consequently higher catalytic activity for the methane oxidation reaction. Nevertheless, these samples quickly deactivated under reaction. This should be attributed to the sintering of small Pd particle into larger one due to the weak interaction between the organic precursor and the support rather than the decomposition of PdO to Pd.[83, 133]

It is quite difficult to compare the catalytic performance of materials reported in the literatures for combustion of CH_4 since the activity tests were conducted under different operation parameters such as the concentration of feed gas and gas hour space velocity (GHSV). Concerning to similar reaction conditions, we tried to draw some conclusions in terms of what are the best performing material among all those listed and discuss underlined reason. Metal-supported on hexaaluminate catalysts, such as $2\%Pd/LaMnAl_{11}O_{19}$[47] and $10\%CeO_2/BaAl_{12}O_{19}$[51], showed interesting low-temperature activity with $T_{10\%}$ of about 400 °C, compared to 510 °C and 450 °C for $BaMnAl_{11}O_{19}$[45] and $LaMnAl_{11}O_{19}$[82] catalysts, respectively. However, the CH_4 conversion over $2\%Pd/LaMnAl_{11}O_{19}$ dropped from 93% to 59% during 100 h run, indicating its poor stability. Although high dispersion CeO_2 nanoparticles on $BaAl_{12}O_{19}$ hexaaluminate were preserved even after calcination at 1100 °C in the presence of H_2O, the stability test under real reaction conditions were not carried out for $10\%CeO_2/BaAl_{12}O_{19}$ catalyst. Besides metal-supported hexaaluminate, $LaFeAl_{11}O_{19}$ with specific surface area of 46 m^2/g prepared by RM combined with SCD also showed high activity with $T_{10\%}$ and $T_{90\%}$ of 400 °C and 590 °C, respectively.[87] This was due to the improvement of mobility of lattice oxygen resulted from the enhancement of specific surface area. $LaMn_3Al_9O_{19}$[82] and $LaMg_{0.5}Mn_{0.5}Al_{11}O_{19}$[13] exhibited improved activity compared with $LaMnAl_{11}O_{19}$. This was attributed to more Mn ions stabilized in high oxidation state which was generally regarded to be the active sites for the combustion of CH_4. Additionally, CH_4 conversion kept constant during 100 h of time on stream, indicating that their outstanding thermal stability under reaction conditions.[13, 47]

4.2 Partial oxidation and dry (CO_2) reforming of CH_4 to syngas ($CO+H_2$)

The catalytic conversion of CH_4 to syngas, such as partial oxidation of CH_4 (POM) and dry (CO_2) reforming of CH_4 (DRM), has attracted a considerable interest in the last two decades for the chemical utilization of natural gas.[40] It was found that nickel-based catalysts showed high activity, but they deactivated more easily due to sintering of both the active metal and the support oxide as well as the deposition of carbon. Strong interaction between Ni and support can improve the activity and suppress the carbon deposition.[46] In addition, the formation of elemental carbon on

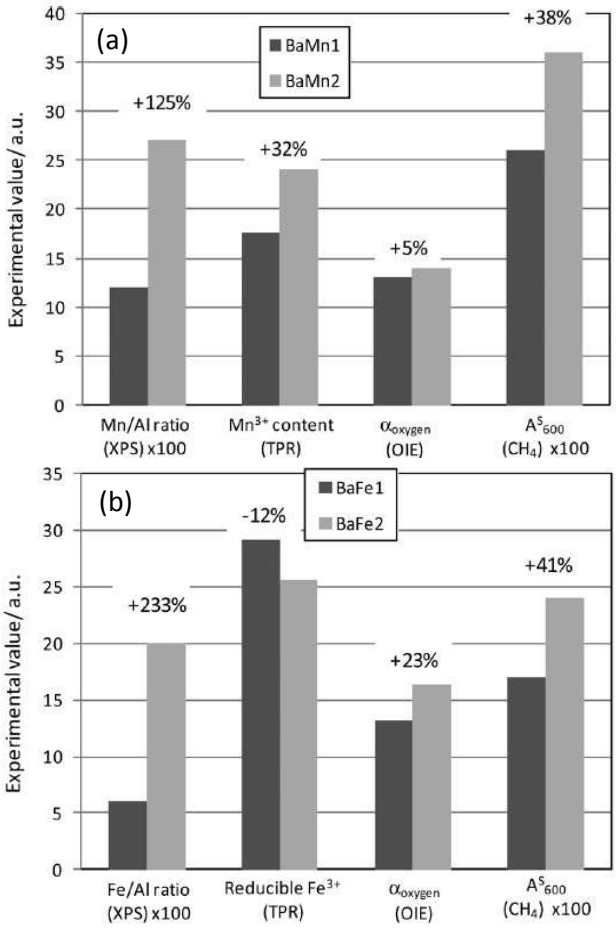

Fig. 11 Impact of the substitution degree on: transition metal surface content determined by XPS; reducible metal content as evaluated by TPR-H_2; oxygen mobility measured by oxygen isotopic exchange (OIE); specific activity for the CH_4 oxidation reaction (A^s_{600}: mmol of CH_4 converted at 600 °C per unit of surface), (a) Mn- and (b) Fe-substituted hexaaluminates.[114]

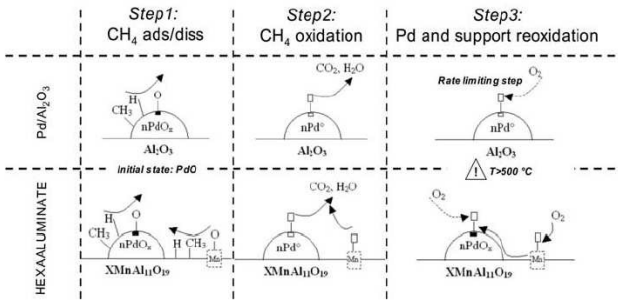

Fig. 12 Proposed scheme of the oxygen transfer between palladium and manganese from the support.[65]

the catalyst surface has been shown to be more rapid on larger metal clusters.[134] The introduction of active Ni species into the lattice of hexaaluminates with high thermal stability will limit the sintering and loss of Ni species at high temperature. Moreover, Ni species show high dispersion in the framework of hexaaluminates and strong interaction with the support, thereby reducing carbon deposition. It is generally accepted that Ni^0 nanoparticles produced from the reduction of Ni-substituted hexaaluminates are highly active for the formation of syngas.[107, 117, 134]. Thus, pre-reduction treatment to hexaaluminate catalysts prior to reaction is desirable to prevent the combustion of CH_4 from occurring.[88, 101, 104, 106]

Chu et al.[104] prepared $BaNi_yAl_{12-y}O_{19-\delta}$ (y=0.3, 0.6, 0.9, 1) using the decomposition of nitrates and tested their catalytic performances for POM. Besides a little amount of the $BaAl_2O_4$ phase, all the samples presented MP structure and no nickel oxide was observed, indicating high dispersion of Ni species. These catalysts showed high activity and selectivity with the CH_4 conversion of ~92% and CO selectivity of ~95% at 850 °C. Especially, the catalysts exhibited excellent ability to suppress carbon deposition and loss of nickel so that the catalytic performances were constant after 100 h of time on stream, which was attributed to the strong interaction between Ni and the neighboring atoms. Utaka et al.[88] compared the activity of Ni/Al_2O_3, hexaaluminate-type $BaNi_xAl_{12-x}O_{19-\alpha}$ (x=0.25, 0.5 and 1) and found that the latter calcined at 1400 °C exhibited more stable and higher activity than the former calcined at 1000 °C. The $BaNiAl_{11}O_{19-\alpha}$ (calcined at 1400 °C) catalyst reduced at 1000 °C demonstrated higher activity than $BaNiAl_{11}O_{19-\alpha}$ (1200 °C) reduced at 800 °C, which originated from the production of a Ni-rich surface and highly dispersed Ni species derived from hexaaluminate crystal. Gardner et al.[134] found that POM over $Ba_{0.75}Ni_yAl_{12-y}O_{19-\delta}$ (x=0.2, 0.4, 0.6, 0.8 and 1) catalysts produced two distinct zones in the post-run catalyst bed, readily identified by the color difference. At the inlet of the catalyst bed, Ni^{2+} was present in the hexaaluminate lattice. In the downstream portion, small Ni clusters was supported on the hexaaluminate catalyst, which corresponded to a reaction sequence wherein the oxidation of CH_4 proceeded at the inlet until all oxygen was reacted, followed by the reaction of CO_2 and H_2O with un-reacted CH_4, and its derivatives, to produce the final syngas mixture, as presented in Fig. 13.

As for the DRM, $LaNi_xAl_{12-x}O_{19}$ (0<x<1),[103, 107] $BaNi_xAl_{12-x}O_{19}$ (0<x<1)[9] and $ANiAl_{11}O_{19}$ (A=Ca, Sr, Ba, La, Ce, Pr)[100-102, 106] hexaaluminate systems have been reported. The maximum x value for the formation of pure hexaaluminate phase was x=1. The activity increased with Ni substitution degree but the amount of carbon produced also enhanced.[9, 107] The nature of large cations in the mirror plane strongly affected the reducibility and activity of catalysts.[106] For example, La-modified hexaaluminate $LaNiAl_{11}O_{19-\delta}$ gave the lowest reduction temperature than $ANiAl_{11}O_{19}$ (A=Ca, Sr, Ba). When the alkaline earth metals (Ba, Sr, Ca) were employed, reduction temperature decreased with an increase in ionic radius of large cations.[106] Zhang et al.[101] investigated the effect of Pr on the structure and catalytic performances of $LaNiAl_{11}O_{19}$. The addition of Pr improved the dispersion of Ni after reduction and the electronic transformation between La ions and Ni ions to maintain Ni at lower valence, which promoted the activation of CH_4. Additionally, more Ni ions located in octahedral sites, which was easily reduced to metallic Ni. All these effects contributed to the enhancement of catalytic activity of the Pr modified La-hexaaluminates. However, the understanding of the underlying reduction mechanism for thermally stable Ni^0 nanoparticles from nickel-containing hexaaluminates and the formation mechanisms for the genesis of such materials is missing. Roussière et al.[117] proposed growth mechanism of the Ni^0 nanoparticles (NPs) on the hexaaluminate phase to understand the stability of the metallic Ni nanoparticles (NPs) under reductive conditions, as shown in Fig. 14. The amount of Ni in $ANi_yAl_{12-y}O_{19}$ (A=Ba, La, Sr; 0<y≤1) should be as low as y= 0.25 in order to control the textural growth of metallic Ni^0 NPs (tetrahedra) and their high dispersion in the form of very small Ni NPs. In addition, the calcination temperature should be kept adequate (1250 °C for 2.5 h) to maintain sufficient concentration of surface defect sites. Otherwise, excess Ni yielded larger Ni^0 NPs (sphericity) on the impurity phase, which resulted in the carbon deposition and was therefore undesired.[116]

4.3 Decomposition of N_2O

4.3.1 The abatement of N_2O. N_2O mitigation is an important topic due to its greenhouse effect in our atmosphere. Nitric acid plants currently represent the largest single source of N_2O in the

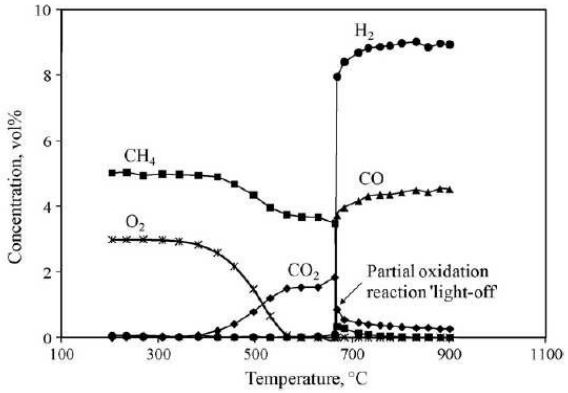

Fig. 13 Exit concentrations for the temperature programmed POM over $Ba_{0.75}Ni_{0.8}Al_{11.2}O_{19-\delta}$.[134] (Reaction conditions: 5%CH_4 and 2.5% O_2 in N_2, GHSV=25000 $cm^3 \cdot h^{-1} \cdot g^{-1}$).

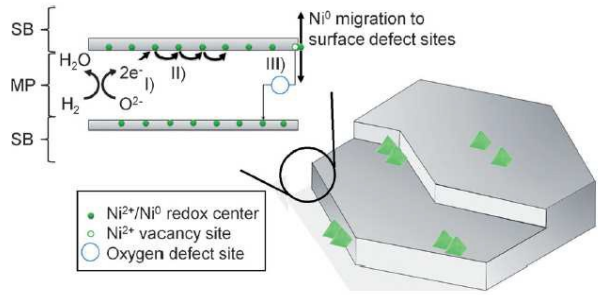

Fig. 14 The proposed reduction mechanism. After O^{2-} removal from the mirror plane (I), the electrons left from H_2 oxidation migrate (II) up to reduce Ni on the outer surface (III). The Ni^0 migrates to surface defect sites to minimize its energy. (SB, spinel block; MP, mirror plane.)[116]

chemical industry (400 kt of N_2O/year), formed as a byproduct of ammonia oxidation over the Pt-Rh alloy gauzes. Direct decomposition of N_2O below the noble metal gauzes in the ammonia burner (process-gas decomposition) is the most cost-effective abatement measure for the existing nitric acid plants. However, reaction occurred at high temperature (1073-1173 K) and in a wet oxidizing atmosphere, which requires the chemical stability of catalysts to avoid volatilization and solid-state reactions between active phase and support leading to catalyst deterioration. Attending to these requirements, metal-substituted hexaaluminates can be considered as promising candidates toward active and durable catalysts for high-temperature N_2O decomposition. Major contributions come from Pérez-Ramírezresearch group.[10, 69, 112, 135, 136] They evaluated the activity of $ABAl_{12}O_{19}$ (A=La, Ba; B=Mn, Fe and Ni) hexaaluminates for decomposition of N_2O under simulating the conditions at the outlet of the noble metal (Pt-Rh) gauzes in ammonia burners of nitric acid plants. Fe- and Mn-containing hexaaluminates showed the highest activities while the Ni-containing catalysts are significantly less active, compared to the non-substituted hexaaluminate.[10] They also investigated the effect of feed compositions on the catalytic performances. As shown in Fig. 15, NO had no effect on the activity while the presence of O_2, H_2O and N_2O+NO+O_2 (referred to as 'all' in Fig. 15) inhibited the activity, which could be attributed to competitive adsorption over active sites in the catalysts.[136] Then, Santiago et al.[112] obtained specific surface area of $LaFeAl_{11}O_{19}$ hexaaluminates increased up to a factor of 25 using a carbon-assisted templating route. Fig. 16 presented the TEM images and pictorial schemes of catalysts at different stages during preparation of $LaFe_{11}O_{19}$ without and with carbon template. In the conventional co-precipitation method, calcination at 700 °C resulted in the development of spherical-like nanoparticles in the precipitation into platelets (Fig. 16 (b), left), which extensively agglomerated to hexaaluminate particles with a broad size distribution in the range of 40-110 nm (Fig. 16 (d), left). In comparison, finely dispersed hexaaluminate particles were obtained by carbon templating method (Fig. 16 (d), right), which originated from the growth of small crystallites at the carbon surface in the composite and the vigorous combustion of the template through fragmentation of the oxide layer deposited on the template. The enhanced catalytic activity and high time-on-stream stability of the templated hexaaluminates was demonstrated in the direct N_2O decomposition using model and simulated feed mixtures. Kondratenko et al.[135] studied mechanistic and kinetic aspects of N_2O decomposition over $BaFeAl_{11}O_{19}$ hexaaluminate in the temporal analysis of products (TAP) reactor and compared with those over Fe-MFI zeolites to identify the factors governing the different catalytic performance. They proposed the reaction pathways over $BaFeAl_{11}O_{19}$ as followed:[135]

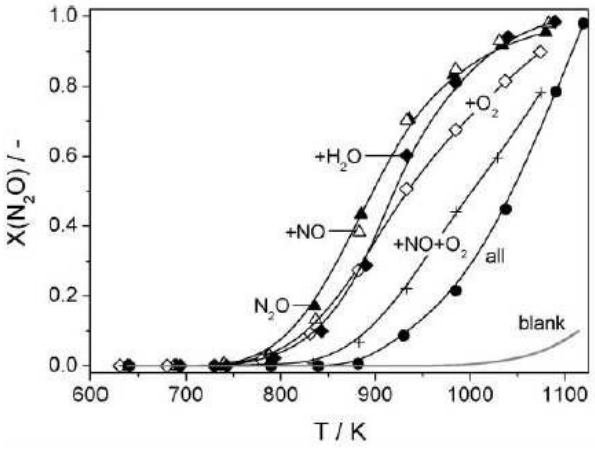

Fig. 15 N_2O conversion versus temperature over Ba-Fe-Al hexaaluminate in feed mixtures with N_2O and additional components at the outlet of the Pt-Rh gauzes in ammonia burners.[136] (Reaction conditions: 1500 ppm N_2O, 10 % O_2, 1.5% NO and 10% H_2O in He; GHSV=30000 $ml \cdot h^{-1} \cdot g^{-1}$).

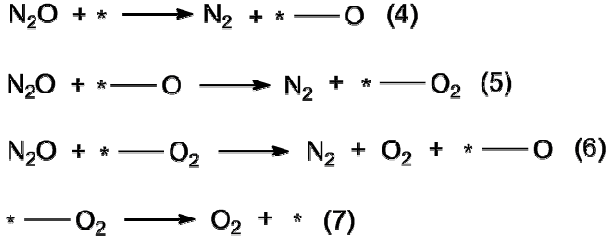

According to this reaction mechanism, gas-phase N_2 and O_2 were simultaneously formed upon interaction of gas-phase N_2O with a bi-atomic surface oxygen *-O_2 species. This was different from Fe-MFI where the formation of O_2 limited the overall rate of N_2O decomposition. Despite the easier desorption of O_2, $BaFeAl_{11}O_{19}$ was less active than Fe-MFI zeolites below 700 °C due to the low coverage of *-O_2 which was strongly influenced by the degree of isolation of Fe species, e. g. the higher degree of Fe isolation in the catalyst, the lower activity for N_2O decomposition.

4.3.2 N_2O as propellant. On the other hand, nitrous oxide (N_2O) is considered to be a promising green propellant due to a number of

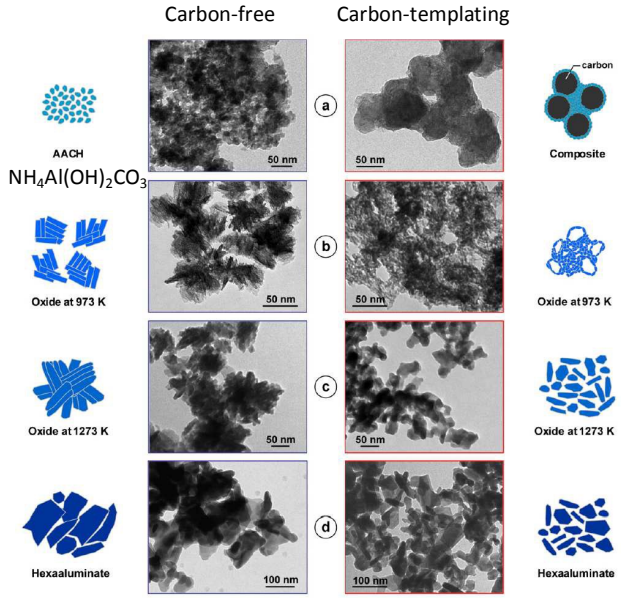

Fig. 16 TEM images and pictorial schemes of catalysts at different stages during preparation of $LaFe_{11}O_{19}$ without and with carbon template.[112]

advantages, such as system simplicity and low cost associated with the extremely low toxicity, self-pressurizing and compatibility of N_2O with common construction materials. However, in view of the extreme operating conditions of N_2O decomposition applicable in the propulsion systems (vol_{N2O} % = 30-100 %, T > 1000 °C, E_a ≈ 250 kJ/mol), a suitable catalyst which must be able to initiate the decomposition of N_2O at a low temperature and to survive at very high temperatures are required.

Our group for the first time developed a novel $BaIr_yFe_{1-y}Al_{11}O_{19}$ (y=0.2, 0.5 and 0.8) (BIFA) catalysts which exhibited not only high activity but also excellent stability.[3, 95] As shown in Fig. 17, N_2O decomposition started at about 323 °C and the full N_2O conversion was obtained at 450 °C (Fig. 17 (a)). BIFA could retain 100% N_2O conversion at 500 °C for more than 26 h without any decay, in contrast with the rapid deactivation over the Ir/Al_2O_3 (Fig. 17 (b)). It was claimed that Ir species in the hexaaluminate lattice were active sites whereas those outside the hexaaluminate crystalline framework were susceptible to sintering and less active for this reaction. The addition of Fe component facilitated the incorporation of Ir into the hexaaluminate framework[95]. Then we identified the crystallographic sites of Fe and Ir in $BaIr_{0.2}FeAl_{10.8}O_{19}$ hexaaluminate by Rietveld refinement combined with ^{57}Fe Mössbauer spectroscopy.[68] Fe occupied both the symmetric tetrahedral Al(2) sites in the spinel block and the distorted tetrahedral interstitial Al(5) sites in the mirror plane while Ir ions only occupied the distorted tetrahedral interstitial Al(5) sites in the loosely packed mirror plane, which originated from Ir ions in oxidic entities dispersed on the Ba-modified γ-Al_2O_3 in the precursor. Ir ions in the Al(5) sites were highly active for N_2O decomposition. We also determined the crystallographic sites of Ir in $BaIr_xFe_{12-x}O_{19}$ (x=0.1, 0.4 and 0.6) through the analysis of Fe occupancy in the

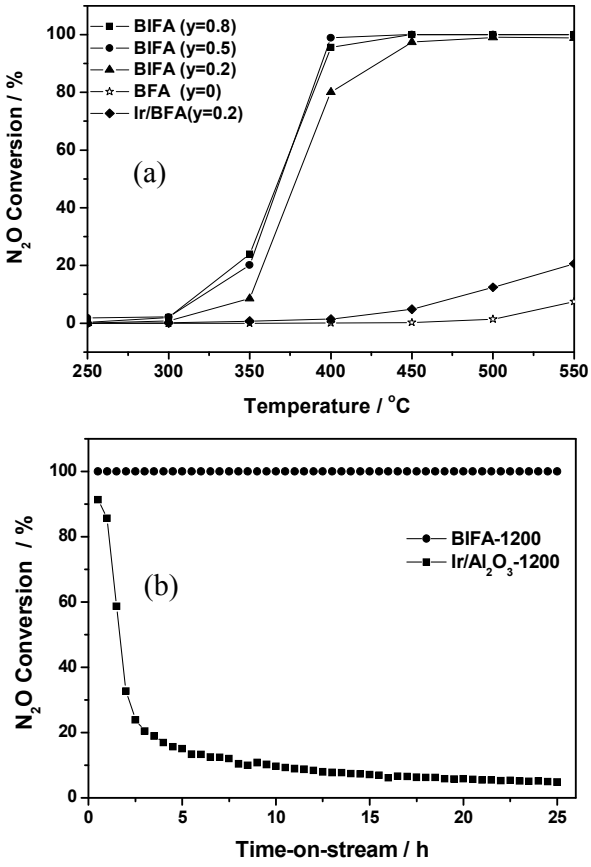

Fig. 17 Effect of Ir contents on the catalytic performances over BIFA catalysts (a), evolution of N_2O conversions at 500 °C as a function of the time-on-stream over BIFA-1200 (y=0.2) and Ir/Al_2O_3-1200 catalysts (b).[3] (Reaction conditions: 30% N_2O in Ar, GHSV=30000 $ml \cdot h^{-1} \cdot g^{-1}$)

matrix by sensitive ^{57}Fe Mössbauer spectroscopy.[11] Framework iridium preferentially occupied the octahedral sites in the order of 2a (Al(4)), 12k (Al(1)), and $4f_2$ (Al(3)) as increasing x value. When x = 0.1 and 0.4, the substitution of Ir for Fe^{3+} occurred in the 2a and 12k sites in the rigid spinel block with a comparable N_2O decomposition activity, while the substitution in the $4f_2$ sites in the mirror plane at x = 0.6 resulted in a remarkable enhancement of activity, indicating that Ir ions in the octahedral $4f_2$ sites in the loosely packed mirror plane were highly active for N_2O decomposition. Inspired by BIFA systems that Ir showed strong interaction with hexaaluminate support and high dispersion thereby inhibiting the sintering and loss of Ir, we extended the noble metal to Ru which is regarded to be the most volatile compared with Ir, Pd, Pt and Rh and proposed the stabilization mechanism of Ru in the Fe-substituted hexaaluminates lattice.[96] It was found that the evaporation of Ru species under high-temperature condition (1100–1200 °C) could be effectively suppressed by the addition of Fe in the hexaaluminate precursor due to the formation of intermediate stable $BaRuO_3$ phase, thus allowed more Ru species entering into the final sintering- resistant hexaaluminate lattice after high-temperature treatment. Ru ions

in the hexaaluminate structure occupied the distorted tetrahedral interstitial Al(5) sites in the loosely packed mirror plane, which originated from Ru species in oxidic entities dispersed on the Ba-modified -Al_2O_3 and the intermediate $BaRuO_3$ in the precursors. Ru ions in the Al(5) sites were responsible for their high activity for N_2O decomposition.

The good performance of metals-substituted hexaaluminates is because the active metals can be stabilized in the framework of heat-resistance hexaaluminates. However, the stabilization mechanism of metal ions was still not clear, which was very important for understanding the final metal chemical state in the target hexaaluminate phase and thus the effects on the catalytic properties. This may be due to the complex high-temperature solid-state reaction for the formation of hexaaluminate, which is very difficult to be characterized. To answer this question, we employed Fe as a probe to investigate the local environments of substituted transition metal ions in hexaaluminates by exploring the evolution of Fe from amorphous precursor to Fe-substituted barium hexaaluminate using Rietveld refinement and Mössbauer spectroscopy.[18, 31, 68] As shown in Fig. 18, Fe^{3+} ions originated from oxidic entities dispersed on Ba-modified γ-Al_2O_3 mainly entered into the sites in the loosely packed mirror plane of the hexaaluminates. In particular, Fe^{3+} ions at low concentration preferentially entered into the distorted tetrahedral Al(5) sites of β_l-Al_2O_3 phase, while Fe^{3+} ions at high concentration mainly entered into the distorted trigonal bipyramidal Al(5) and octahedral Al(3) sites with large spaces in the MP phase. Meanwhile, tetrahedral Fe^{3+} ions in intermediate spinel-type $BaAl_2O_4$ preferentially entered into the tetrahedral Al(2) sites in the spinel block of hexaaluminates. We also attempted to correlate the intrinsic activities of $BF_xAl_{12-x}O_{19}$ (x=1-4) catalysts at 550 °C with the number of Fe^{3+} ions in different crystallographic sites of β_l -Al_2O_3 and MP phases. As shown in Fig. 19, Fe^{3+} ions both in the β_l -Al_2O_3 and MP structure of $BF_xAl_{12-x}O_{19}$ (x=1-4) catalysts were responsible for N_2O decomposition. Combined with H_2-reduced Mössbauer results, we could conclude that Fe ions in the Al(5) sites of β_l -Al_2O_3 and the Al(3) sites of MP phase in the mirror plane should be highly active for N_2O decomposition.

Compared with Ba-hexaaluminates with β-Al_2O_3 structure, La-hexaaluminates with MP structure possesses more substituted Al sites in the mirror plane. In addition, it was reported that the

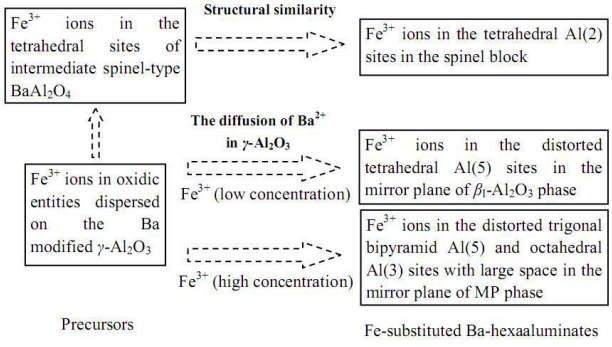

Fig. 18 The evolution schematic diagram of Fe from precursors to different crystallographic sites of Fe-substituted $BaFe_xAl_{12-x}O_{19}$ (x=1-4) hexaaluminates. [68]

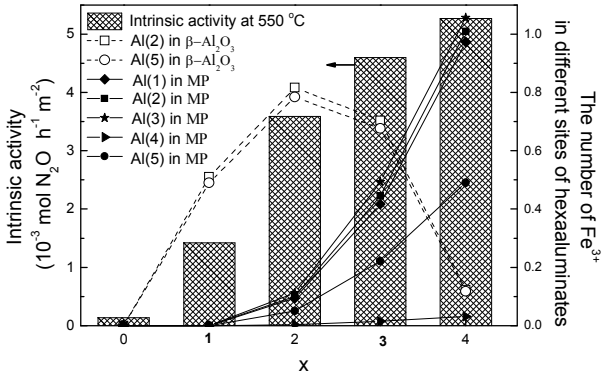

Fig. 19 The intrinsic activity at 550 °C and the number of Fe^{3+} in different crystallographic sites of both β_l-Al_2O_3 and MP catalysts.[68]

formation routes for β-Al_2O_3 and MP structure were different,[127, 137] which probably led to a distinct substituting mechanism of transition metals in the La-hexaaluminates. To this end, we investigated Fe-substituted La-hexaaluminates with a concentration on the evolution of the chemical state and localization of Fe ions during thermal treatment monitored by ^{57}Fe Mössbauer spectroscopy (Fig. 20).[32, 86] Fe^{3+} ions originating from the initial α-Fe_2O_3 mainly incorporated into the tetrahedral Al(2) and Al(5) sites while those in the octahedral sites of perovskite-type $LaFeO_3$ intermediates preferentially accommodated in the octahedral Al(3) sites in the mirror plane of La-hexaaluminates. Correlation of normalized rates of the catalysts at 500 °C with the occupancy of Fe ions in different Al crystallographic sites of the MP phase indicated that Fe^{3+} ions in the Al(3) and Al(5) sites were highly active for N_2O decomposition.

Although noble metals-substituted hexaaluminates showed high activity and stability, quite limited amount (usually less than 0.2 metal ions) could enter the framework of hexaaluminates. This resulted in relatively high initiation temperature of N_2O decomposition over hexaaluminates compared with supported noble metals. To solve this problem, we developed a two-bed reactor,[137, 138] wherein highly active Ir/Al_2O_3 catalyst constituted the front bed while the back bed composed of more thermally

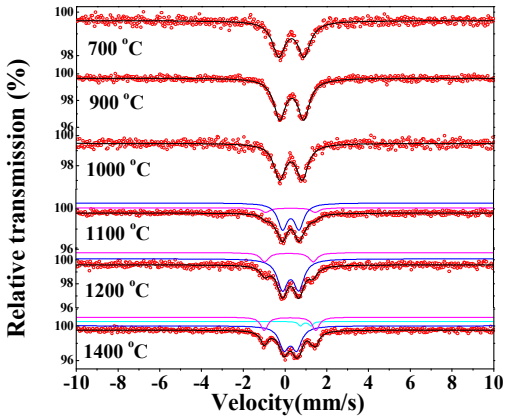

Fig. 20 ^{57}Fe Mössbauer spectra of $LaFeAl_{11}O_{19}$-t (t represents calcination temperature).[86]

stable Mn-substituted hexaaluminates. The activity tests for the two-bed catalysts in a thruster exhibited that they worked continuously for 500 s in the first run and could proceed successfully for 6 cycles. Mn content in the back-bed catalyst after the sixth reaction remained essentially the same as that of the fresh catalyst (6.9 wt% vs. 6.7 wt%), strongly demonstrated that the Mn-substituted Ba-hexaaluminate is a promising candidate as the back-bed catalyst for N_2O propellant decomposition.[18]

5. Conclusions and outlook

Hexaaluminates possess layered structure, consisting of alternate stacking closely packed spinel blocks along the c axis and loosely packed mirror planes in which large cations are resided. This endows hexaaluminates remarkable resistance to sintering and thermal shock so that stable phase composition can be maintained up to 1600 ^{o}C. In addition, aluminum cations in both the spinel block and mirror planes can be partial or completely substituted by transition or noble metals, giving rise to a variety of redox centers, which plays significant roles in heterogeneous catalysis. Active species in the loosely packed mirror plane, a preferentially exposed surface and path are more easily moved and diffused, thus greatly facilitating the adsorption and desorption of reactants. These unique properties of hexaaluminates make them promising materials for numerous applications. For three decades, considerable developments have been made on hexaaluminates-based materials for their applications in heterogeneous catalysis, and good performances have been reported in terms of their capabilities to efficiently catalyze combustion of CH_4, POM, DRM and decomposition of N_2O, etc.

However, the specific surface area of hexaaluminates is low, typically in the range of 10-20 m^2/g arising from high crystallization temperature generally higher than 1200 ^{o}C accompanied by grain growth. During past 15 years, considerable efforts were made to prepare high-surface hexaaluminates, specific surface areas being reached up to 100 m^2/g or more. These are ascribed to the decrease of the crystallization temperature by improving chemical homogeneity of precursor, and suppressing grain-growth during crystallization. In addition, non-conventional drying methods, e. g. freeze drying and supercritical drying which have to be operated under oxygen and moisture-free conditions are adopted to maintain the homogeneous mixing of components. Evidently, it is impossible to produce hexaaluminates in large scale by such preparations under stringent conditions and using expensive and toxic agents and reactants. Therefore, future investigations should concern the preparation of precursor by simplifying the operation and using inexpensive and environmental benign raw materials. Great efforts will also be made to separate the grain-growth and crystallization process. Thus, post-treatment may be conducted on precursors such as carbon coating to avoid the growth of particles during crystallization. The calcination of precursor under inert atmosphere for crystallization, followed by the removal of templating agents such as carbon black may also efficiently suppress the agglomeration of particles and improve the specific surface area, as stated by Gao et al.[111]

In spite of the exceptional thermal stability of hexaaluminates, light-off activity is relatively low compared with noble metals and other metal oxide catalysts such as perovskite and spinel, which limits its wide application in heterogeneous catalysis. Two possible reasons are as follows. (ⅰ) only a little amount of noble metals (<2%) can substitute aluminum ions to enter the lattice of hexaaluminate, which leads to the limited accessible active sites (redox centers). (ⅱ) low specific surface area due to high-temperature calcination results in the poor dispersion of active species when supported on hexaaluminates. Future studies will be focus on the preparation of high dispersion noble metal nanoparticles (NPs) on the large-surface hexaaluminates. Roussière et al.[116, 117] found that small Ni^0 NPs can be stabilized on the surface defect sites of hexaaluminate platelets by controlling the Ni content lower than y=0.25 and calcination temperature at 1200 ^{o}C. Inspired by this work, highly dispersed noble metal NPs derived from the substituted hexaaluminates with enhanced specific surface area may be obtained. Compared to conventional wet impregnation: (1) high dispersion of noble metal ions in the hexaaluminates structure will be beneficial for the good dispersion of the active center after reducing; (2) oxygen within the mirror plane will be preferentially reduced, exposing active noble metal sites in this region, which may be stabilized by their lattice configuration matching with the quasi cubic close packed lattice of the O^{2-} anions inside the spinel blocks of hexaaluminates. (3) metal alloys may form during reducing noble and transition metals co-substituted hexaaluminates, which must influence the structure of noble metal NPs thus the activity for the targeted reactions. Investigations on this area will also develop the fundamental understanding the surface properties of hexaaluminates, which is lacking but important in heterogeneous catalysis.

Although a great deal of work has been achieved in the understanding the nature of active sites in the hexaaluminate structure, investigations are far from over. With the development of characterization methods, computational chemistry, catalyst synthesis, future research is expected to address: (ⅰ) interaction between reactants and active sites and the evolution of active centers (intermediates) along reaction; (ⅱ) rate limited step and reaction pathway. (ⅲ) correlation of substitution, oxygen vacancies, active oxygen species and catalytic performances.

Acknowledgements

Financial support was provided by the National Science Foundation of China (NSFC) grants (21076211; 21406225) and Postdoctoral Science Foundation of China (2014M561261).

Notes and references

1. N. Iyi, S. Takekawa and S. Kimura, *J. Solid State Chem.*, 1989, **83**, 8-19.
2. L. Lietti, C. Cristiani, G. Groppi and P. Forzatti, *Catal. Today*, 2000, **59**, 191-204.
3. S. Zhu, X. Wang, A. Wang, Y. Cong and T. Zhang, *Chem. Commun.*, 2007, 1695-1697.
4. R. Kikuchi, Y. Iwasa, T. Takeguchi and K. Eguchi, *Appl. Catal. A*, 2005, **281**, 61-67.

5. R. S. Roth and S. Hasko, *J. Am. Ceram. Soc.*, 1958, **41**, 146-146.
6. M. Machida, K. Eguchi and H. Arai, *J. Catal.*, 1987, **103**, 385-393.
7. H. Arai and M. Machida, *Appl. Catal. A*, 1996, **138**, 161-176.
8. J. Schicks, D. Neumann, U. Specht and G. Veser, *Catal. Today*, 2003, **81**, 287-296.
9. T. H. Gardner, J. J. Spivey, E. L. Kugler and D. Pakhare, *Appl. Catal. A*, 2013, **455**, 129-136.
10. M. Santiago and J. Perez-Ramirez, *Environ. Sci. Technol.*, 2007, **41**, 1704-1709.
11. Y. Zhu, X. Wang, Y. Zhang, J. Wang, Y. Huang, C. Kappenstein and T. Zhang, *Appl. Catal. A*, 2011, **409**, 194-201.
12. X. L. Chen, B. L. Zou, Y. Wang, H. M. Ma and X. Q. Cao, *J. Therm. Spray Technol.*, 2011, **20**, 1328-1338.
13. F. Teng, Y. Man, S. Liang, G. Buergen, Y. Zhu, W. Han, P. Xu, G. Xiong and Z. Tian, *J. Non-Cryst. Solids*, 2007, **353**, 4806-4812.
14. J. G. Park and A. N. Cormack, *J. Solid State Chem.*, 1996, **121**, 278-290.
15. S. Laassiri, D. Duprez, S. Royer and H. Alamdari, *Catal. Sci. Technol.*, 2011, **1**, 1124-1127.
16. L. Lietti, C. Ramella, G. Groppi and P. Forzatti, *Appl. Catal. B*, 1999, **21**, 89-101.
17. G. Groppi, A. Belloli, E. Tronconi and P. Forzatti, *Catal. Today*, 1996, **29**, 403-407.
18. M. Tian, A. Wang, X. Wang, Y. Zhu and T. Zhang, *Appl. Catal. B*, 2009, **92**, 437-444.
19. N. Iyi, Z. Inoue, S. Takekawa and S. Kimura, *J. Solid State Chem.*, 1984, **54**, 70-77.
20. A. J. Lindop, C. Matthews and D. W. Goodwin, *Acta Crystallogr. Sect. B*, 1975, **31**, 2940-2941.
21. A. L. N. Stevels and A. D. M. Schrama-de Pauw, *J. Electrochem. Soc.*, 1976, **123**, 691-697.
22. S. Kimura, E. Bannai and I. Shindo, *Mater. Res. Bull.*, 1982, **17**, 209-215.
23. N. Iyi, Z. Inoue, S. Takekawa and S. Kimura, *J. Solid State Chem.*, 1985, **60**, 41-50.
24. G. Brunton, *Acta Crystallogr. Sect. B*, 1971, **27**, 1826-1834.
25. P. D. Dernier and J. P. Remeika, *J. Solid State Chem.*, 1976, **17**, 245-253.
26. W. L. Roth, *J. Solid State Chem.*, 1972, **4**, 60-75.
27. W. L. Roth, F. Reidinger and S. Laplaca, *Superionic Conductors*, Plenum, New York, 1977.
28. J. C. Wang, *J. Chem. Phys.*, 1980, **73**, 5786-5795.
29. M. Machida, K. Eguchi and H. Arai, *J. Am. Ceram. Soc.*, 1988, **71**, 1142-1147.
30. M. Machida, A. Sato, T. Kijima, H. Inoue, K. Eguchi and H. Arai, *Catal. Today*, 1995, **26**, 239-245.
31. Y. Zhu, X. Wang, G. Wu, Y. Huang, Y. Zhang, J. Wang and T. Zhang, *J. Phys. Chem. C*, 2012, **116**, 671-680.
32. Y. Zhang, X. Wang, Y. Zhu, X. Liu and T. Zhang, *J. Phys. Chem. C*, 2014, **118**, 10792-10804.
33. M. Machida, A. Sato, M. Murakami, T. Kijima and H. Arai, *J. Catal.*, 1995, **157**, 713-720.
34. S. Nugroho, Z.-C. Chen, A. Kawasaki and M. O. D. Jarligo, *J. Alloys Compd.*, 2010, **502**, 466-471.
35. P. Artizzu-Duart, J. M. Millet, N. Guilhaume, E. Garbowski and M. Primet, *Catal. Today*, 2000, **59**, 163-177.
36. L. C. Yan and L. T. Thompson, *Appl. Catal. A*, 1998, **171**, 219-228.
37. D. Naoufal, J. M. Millet, E. Garbowski, Y. Brulle and M. Primet, *Catal. Lett.*, 1998, **54**, 141-148.
38. P. Artizzu, N. Guilhaume, E. Garbowski, Y. Brulle and M. Primet, *Catal. Lett.*, 1998, **51**, 69-75.
39. S. Royer, C. Ayrault, C. Carnevillier, F. Epron, P. Marecot and D. Duprez, *Catal. Today*, 2006, **117**, 543-548.
40. L. Majocchi, G. Groppi, C. Cristiani, P. Forzatti, L. Basini and A. Guarinoni, *Catal. Lett.*, 2000, **65**, 49-56.
41. M. Bellotto, G. Artioli, C. Cristiani, P. Forzatti and G. Groppi, *J. Catal.*, 1998, **179**, 597-605.
42. G. Groppi, M. Bellotto, C. Cristiani, P. Forzatti and P. L. Villa, *Appl. Catal. A*, 1993, **104**, 101-108.
43. M. Berg and S. Jaras, *Catal. Today*, 1995, **26**, 223-229.
44. M. V. Bukhtiyarova, A. S. Ivanova, L. M. Plyasova, G. S. Litvak, A. A. Budneva and E. A. Paukshtis, *React. Kinet. Catal. Lett.*, 2008, **93**, 375-387.
45. L. Ma, B. Shi, M. Cui, L. Wang, D. Li and A. Chen, *Sci. China, Ser. B*, 2008, **51**, 211-217.
46. W. L. Chu, W. S. Yang and L. W. Lin, *Catal. Lett.*, 2001, **74**, 139-144.
47. B. W. L. Jang, R. M. Nelson, J. J. Spivey, M. Ocal, R. Oukaci and G. Marcelin, *Catal. Today*, 1999, **47**, 103-113.
48. C. P. B. Quitete, R. C. P. Bittencourt and M. M. V. M. Souza, *Catal. Lett.*, 2015, **145**, 541-548.
49. A. J. Zarur, N. Z. Mehenti, A. T. Heibel and J. Y. Ying, *Langmuir*, 2000, **16**, 9168-9176.
50. A. J. Zarur, H. H. Hwu and J. Y. Ying, *Langmuir*, 2000, **16**, 3042-3049.
51. A. J. Zarur and J. Y. Ying, *Nature*, 2000, **403**, 65-67.
52. P. K. Sahu, B. D. Kulkarni, R. B. Khomane, S. A. Pardhy, U. D. Phalgune, P. Rajmohanan and R. Pasricha, *Chem. Commun.*, 2003, 1876-1877.
53. M. V. Bukhtiyarova, A. S. Ivanova, G. S. Litvak and L. M. Plyasova, *Kinet. Catal.*, 2009, **50**, 824-829.
54. S. Kim, D.-W. Lee, J. Y. Lee, H.-J. Eom, H. J. Lee, I.-H. Cho and W.-Y. Lee, *J. Mol. Catal. A: Chem.*, 2011, **335**, 60-64.
55. C. P. B. Quitete, R. C. P. Bittencourt and M. M. V. M. Souza, *Appl. Catal. A*, 2014, **478**, 234-240.
56. J. Zheng, X. Ren, Y. Song and X. Ge, *Catal. Commun.*, 2009, **10**, 1226-1229.
57. R. Kikuchi, Y. Tanaka, K. Sasaki and K. Eguchi, *Catal. Today*, 2003, **83**, 223-231.
58. J. M. Sohn, S. K. Kang and S. I. Woo, *J. Mol. Catal. A: Chem.*, 2002, **186**, 135-144.
59. S. I. Woo, S. K. Kang and J. M. Sohn, *Appl. Catal. B*, 1998, **18**, 317-324.
60. G. Groppi, F. Assandri, M. Bellotto, C. Cristiani and P. Forzatti, *J. Solid State Chem.*, 1995, **114**, 326-336.
61. T.-F. Yeh, J.-L. Bi, H.-G. Lee, K.-S. Chu and C.-B. Wang, *J. Alloys Compd.*, 2006, **425**, 353-356.
62. T. F. Yeh, H. G. Lee, K. S. Chu and C. B. Wang, *Mater. Sci. Eng. A*, 2004, **384**, 324-330.
63. S. Cimino, R. Nigro, U. Weidmann and R. Holzner, *Fuel Process. Technol.*, 2015, **133**, 1-7.
64. A. Baylet, S. Royer, R. Marecot, J. M. Tatibouet and D. Duprez, *Appl. Catal. B*, 2008, **77**, 237-247.
65. A. Baylet, S. Royer, C. Labrugere, H. Valencia, P. Marecot, J. M. Tatibouet and D. Duprez, *Phys. Chem. Chem. Phys.*, 2008, **10**, 5983-5992.
66. H. Inoue, K. Sekizawa, K. Eguchi and H. Arai, *J. Solid State Chem.*, 1996, **121**, 190-196.
67. P. Artizzu-Duart, Y. Brulle, F. Gaillard, N. Guilhaume and M. Primet, *Catal. Today*, 1999, **54**, 181-190.

68. Y. Zhu, X. Wang, A. Wang, G. Wu, J. Wang and T. Zhang, *J. Catal.*, 2011, **283**, 149-160.
69. M. Santiago, M. A. G. Hevia and J. Perez-Ramirez, *Appl. Catal. B*, 2009, **90**, 83-88.
70. S. G. Lee, H. Lee, C. H. Lee, J. Y. Kwon, H. C. Park, S. S. Hong and S. S. Park, *React. Kinet. Catal. Lett.*, 2005, **86**, 299-306.
71. F. Teng, P. Xu, Z. J. Tian, G. X. Xiong, Y. P. Xu, Z. S. Xu and L. W. Lin, *Green Chem.*, 2005, **7**, 493-499.
72. J. G. Xu, Z. J. Tian, J. W. Wang, Y. P. Xu, Z. S. Wu and L. W. Lin, *React. Kinet. Catal. Lett.*, 2004, **82**, 19-25.
73. L. Lietti, G. Groppi and C. Ramella, *Catal. Lett.*, 1998, **53**, 91-95.
74. M. Astier, E. Garbowski and M. Primet, *Catal. Lett.*, 2004, **95**, 31-37.
75. S. J. Cho, Y. S. Seo, K. S. Song, N. J. Jeong and S. K. Kang, *Appl. Catal. B*, 2001, **30**, 351-357.
76. A. Kantcheva, A. Agiral, O. Samarskaya, M. Stranzenbach and B. Saruhan, *Appl. Surf. Sci.*, 2005, **252**, 1481-1491.
77. J. Zheng, X. Ren, Y. Song and G. Shen, *React. Kinet. Catal. Lett.*, 2007, **92**, 11-17.
78. H. M. J. Kusar, A. G. Ersson and S. G. Jaras, *Appl. Catal. B*, 2003, **45**, 1-11.
79. E. Pocoroba, E. M. Johansson and S. G. Jaras, *Catal. Today*, 2000, **59**, 179-189.
80. E. M. Johansson, K. M. J. Danielsson, E. Pocoroba, E. D. Haralson and S. G. Jaras, *Appl. Catal. A*, 1999, **182**, 199-208.
81. J. G. Xu, Z. J. Tian, J. W. Wang, Y. P. Xu, Z. S. Xu and L. W. Lin, *Korean J. Chem. Eng.*, 2003, **20**, 217-221.
82. J. W. Wang, Z. J. Tian, J. G. Xu, Y. P. Xu, Z. S. Xu and L. W. Lin, *Catal. Today*, 2003, **83**, 213-222.
83. S. A. Yashnik and Z. R. Ismagilov, *Top. Catal.*, 2012, **55**, 818-836.
84. A. Ersson, K. Persson, I. K. Adu and S. G. Jaras, *Catal. Today*, 2006, **112**, 157-160.
85. M. Cui, L. Wang, N. Zhao, Z. Long, D. Li and A. Chen, *J. Rare Earth.*, 2006, **24**, 690-694.
86. Y. Zhang, X. Wang, Y. Zhu, B. Hou, X. Yang, X. Liu, J. Wang, J. Li and T. Zhang, *J. Phys. Chem. C*, 2014, **118**, 1999-2010.
87. Z. Jiang, Z. Hao, J. Su, T. Xiao and P. P. Edwards, *Chem. Commun.*, 2009, 3225-3227.
88. T. Utaka, S. A. Al-Drees, J. Ueda, Y. Iwasa, T. Takeguchi, R. Kikuchi and K. Eguchi, *Appl. Catal. A*, 2003, **247**, 125-131.
89. T. H. Gardner, J. J. Spivey, E. L. Kugler, A. Campos, J. C. Hissam and A. D. Roy, *J. Phys. Chem. C*, 2010, **114**, 7888-7894.
90. H. Kim, S. J. Lee and K. S. Song, *Korean J. Chem. Eng.*, 2007, **24**, 477-480.
91. J. Zheng, X. Ren, Y. Song and X. Ge, *React. Kinet. Catal. Lett.*, 2009, **97**, 109-114.
92. X. Ren, J. Zheng, Y. Song and P. Liu, *Catal. Commun.*, 2008, **9**, 807-810.
93. J. Zheng, X. Ren and Y. Song, *React. Kinet. Catal. Lett.*, 2008, **93**, 3-9.
94. F. Teng, J. G. Xu, Z. J. Tian, J. W. Wang, Y. P. Xu, Z. S. Xu, G. X. Xiong and F. Teng, *Chem. Commun.*, 2004, 1858-1859.
95. S. Zhu, X. Wang, A. Wang and T. Zhang, *Catal. Today*, 2008, **131**, 339-346.
96. Y. Zhang, X. Wang, Y. Zhu and T. Zhang, *Appl. Catal. B*, 2013, **129**, 382-393.
97. P. Jana, P. S. Jayan, S. Mandal and K. Biswas, *J. Cryst. Growth*, 2014, **408**, 7-13.
98. J. D. Zheng, X. G. Ren, Y. J. Song and G. L. Shen, *J. Fuel Chem. Technol.*, 2007, **35**, 117-120.
99. J. D. Zheng, X. G. Ren, Y. J. Song, J. Y. Yu and G. L. Shen, *Chin. Rare Earth.*, 2007, **28**, 40-44.
100. K. Zhang, G. Zhou, J. Li, K. Zhen and T. Cheng, *Catal. Lett.*, 2009, **130**, 246-253.
101. K. Zhang, G. Zhou, J. Li and T. Cheng, *Catal. Commun.*, 2009, **10**, 1816-1820.
102. Y. Liu, T. X. Cheng, D. M. Li, P. B. Jiang, J. X. Wang, W. X. Li, Y. L. Bi and K. J. Zhen, *Catal. Lett.*, 2003, **85**, 101-107.
103. Y. Liu, Z. L. Xu, T. X. Cheng, G. D. Zhou, J. X. Wang, W. X. Li, Y. L. Bi and K. J. Zhen, *Kinet. Catal.*, 2002, **43**, 522-527.
104. W. L. Chu, W. S. Yang and L. W. Lin, *Appl. Catal. A*, 2002, **235**, 39-45.
105. W. Chu, W. Yang and L. Lin, *Chin. J. Catal.*, 2002, **23**, 103-104.
106. Z. L. Xu, M. Zhen, Y. L. Bi and K. J. Zhen, *Catal. Lett.*, 2000, **64**, 157-161.
107. Z. L. Xu, M. Zhen, Y. L. Bi and K. J. Zhen, *Appl. Catal. A*, 2000, **198**, 267-273.
108. H. Zhu, R. J. Kee, J. R. Engel and D. T. Wickham, *Proc. Combust. Inst.*, 2007, **31**, 1965-1972.
109. R. W. Sidwell, H. Y. Zhu, B. A. Kibler, R. J. Kee and D. T. Wickham, *Appl. Catal. A*, 2003, **255**, 279-288.
110. V. Jayaraman, G. Periaswami and T. R. N. Kutty, *Mater. Res. Bull.*, 2008, **43**, 2527-2537.
111. J. Gao, C. Jia, M. Zhang, F. Gu, G. Xu, Z. Zhong and F. Su, *Rsc Advances*, 2013, **3**, 18156-18163.
112. M. Santiago, J. C. Groen and J. Perez-Ramirez, *J. Catal.*, 2008, **257**, 152-162.
113. S. Laassiri, N. Bion, D. Duprez, S. Royer and H. Alamdari, *Phys. Chem. Chem. Phys.*, 2014, **16**, 4050-4060.
114. S. Laassiri, N. Bion, D. Duprez, H. Alamdari and S. Royer, *Catal. Sci. Technol.*, 2013, **3**, 2259-2269.
115. S. Laassiri, N. Bion, F. Can, X. Courtois, D. Duprez, S. Royer and H. Alamdari, *Crystengcomm*, 2012, **14**, 7733-7743.
116. T. Roussiere, L. Schulz, K. M. Schelkle, G. Wasserschaff, A. Milanov, E. Schwab, O. Deutschmann, A. Jentys, J. Lercher and S. A. Schunk, *Chemcatchem*, 2014, **6**, 1447-1452.
117. T. Roussiere, K. M. Schelkle, S. Titlbach, G. Wasserschaff, A. Milanov, G. Cox, E. Schwab, O. Deutschmann, L. Schulz, A. Jentys, J. Lercher and S. A. Schunk, *Chemcatchem*, 2014, **6**, 1438-1446.
118. M. Machida, K. Eguchi and H. Arai, *J. Catal.*, 1989, **120**, 377-386.
119. Z. You, K. Inazu, K.-I. Aika and T. Baba, *J. Catal.*, 2007, **251**, 321-331.
120. K. S. Song, Y. S. Seo, H. K. Yoon and S. J. Cho, *Korean J. Chem. Eng.*, 2003, **20**, 471-475.
121. Q. Yu, L. Yu, Y. Huang, M. Sun, X. Chen, Y. Wang and Q. Zhang, *Rare Metals*, 2006, **25**, 333-336.
122. T. H. Gardner, D. Shekhawat, D. A. Berry, M. W. Smith, M. Salazar and E. L. Kugler, *Appl. Catal. A*, 2007, **323**, 1-8.
123. M. V. Bukhtiyarova, A. S. Ivanova, L. M. Plyasova, G. S. Litvak, V. A. Rogov, V. V. Kaichev, E. M. Slavinskaya, P. A. Kuznetsov and I. A. Polukhina, *Appl. Catal. A*, 2009, **357**, 193-205.
124. D. J. Haynes, A. Campos, M. W. Smith, D. A. Berry, D. Shekhawat and J. J. Spivey, *Catal. Today*, 2010, **154**, 210-216.
125. J. H. Chen, H. Arandiyan, X. Gao and J. H. Li, *Catal. Surv. Asia*, 2015, **19**, 140-171.
126. R. J. H. Voorhoeve, J. P. Remeika, P. E. Freeland and B. T. Matthias, *Science*, 1972, **177**, 353-354.
127. G. Groppi, C. Cristiani and P. Forzatti, *Appl. Catal. B*, 2001, **35**, 137-148.
128. S. Li and X. Wang, *J. Alloys Compd.*, 2007, **432**, 333-337.

129. G. Groppi, C. Cristiani and P. Forzatti, *J. Catal.*, 1997, **168**, 95-103.
130. Y. Yu, L. Wang, M. Cui, Y. Shi, R. Luo and A. Chen, *Rare Metals*, 2011, **30**, 337-342.
131. S. Bai, L. Wang, B. Shi, P. Yang, M. Cui, Z. Long, D. Li and A. Chen, *Sci. China, Ser. B*, 2009, **52**, 31-38.
132. K. Sekizawa, K. Eguchi, H. Widjaja, M. Machida and H. Arai, *Catal. Today*, 1996, **28**, 245-250.
133. A. Baylet, S. Royer, P. Marecot, J. M. Tatibouet and D. Duprez, *Appl. Catal. B*, 2008, **81**, 88-96.
134. T. H. Gardner, J. J. Spivey, A. Campos, J. C. Hissam, E. L. Kugler and A. D. Roy, *Catal. Today*, 2010, **157**, 166-169.
135. E. V. Kondratenko, V. A. Kondratenko, M. Santiago and J. Perez-Ramirez, *Appl. Catal. B*, 2010, **99**, 66-73.
136. J. Perez-Ramirez and M. Santiagoa, *Chem. Commun.*, 2007.
137. J. Lin, Y. Q. Huang, L. Li, B. T. Qiao, X. D. Wang, A. Q. Wang and T. Zhang, *Chem. Eng. J.*, 2011, **168**, 822-826.
138. B. L. Hou, X. D. Wang, T. Li and T. Zhang, *AlChE J.*, 2015, **61**, 1064-1080.

The structure and catalytic applications of hexaaluminates